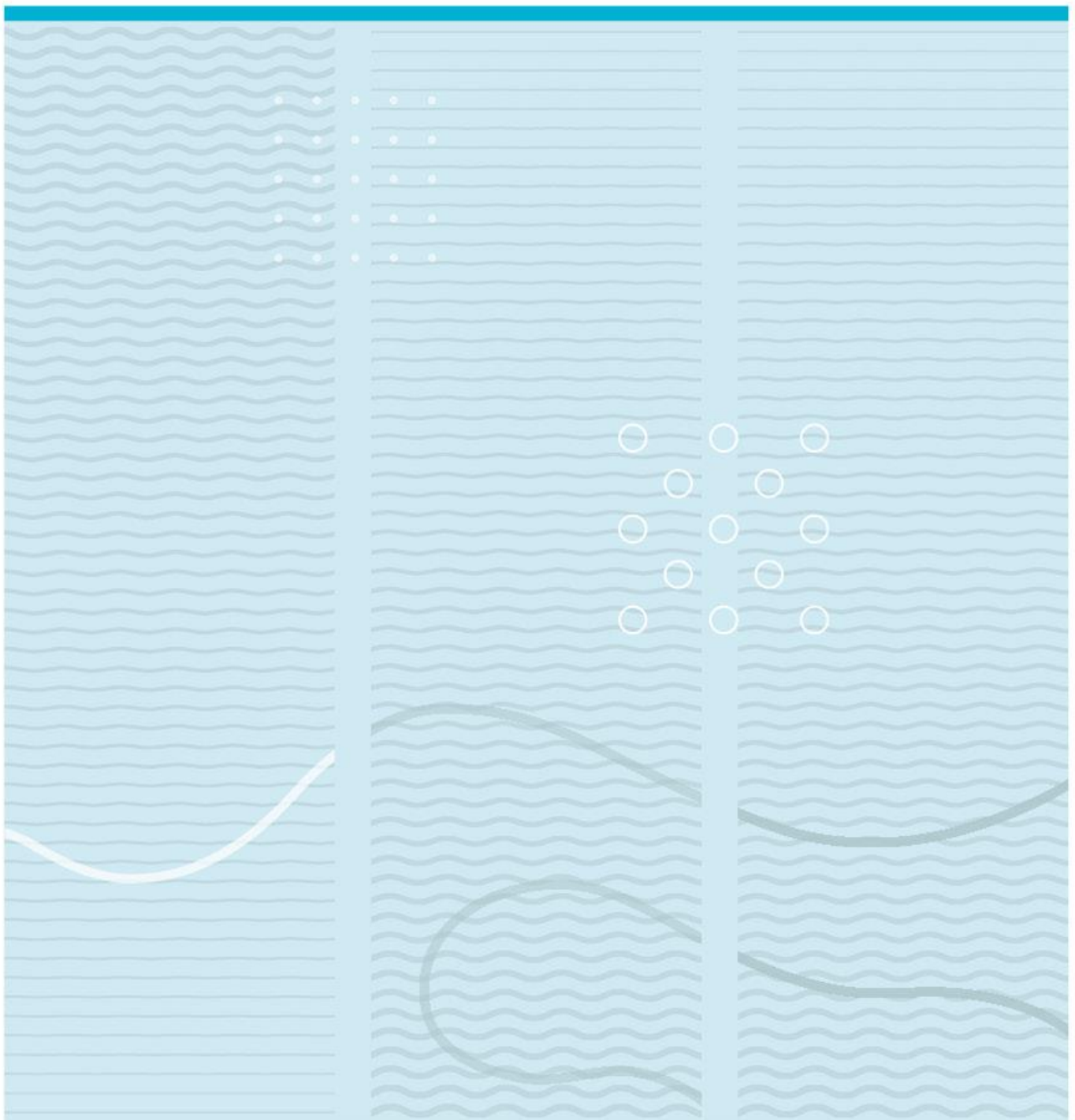


Neda Ghiasi

Supervisor: Erik A. Johannessen

Co Supervisor: Agne Johannessen, Ulrik Hanke

# Modeling of QCM for thin layer immobilization in a liquid environment



University of South-Eastern Norway  
Faculty of Technology, Natural Sciences, and Maritime Sciences  
Department of Microsystems.  
Raveien 215  
NO-3184 Borre, Norway

<http://www.usn.no>

© 20xx <author's name>

# Summary

In this thesis, we develop two models of a quartz crystal microbalance (QCM) to analyze the system's behavior in liquid sensing. These models detail the device response concerning the changes in sensor geometry, surrounding medium, and liquid properties variation.

In the first model, we investigate the electrical equivalent circuit of the ideal device in MATLAB. We can predict the resonant frequency with respect to the sensor's area changes, loading water on top of the sensor, and changes in bulk viscosity and density of the water. The results are reliable and by the experiments.

We simulated another model using finite element analysis (FEM) in COMSOL to examine the system reaction to the changes in sensor radius, liquid loading, and changes in properties of the liquid. In this model, we can check more variables that affect the system operating frequency. The results confirm the previous model achievements with small deviations. Both models provide the grounds for more investigations in the future.

## Nomenclature

A	Area (m <sup>2</sup> )
B	Susceptance (Si)
F	Frequency (Hz)
G	Conductance (Si)
h	Thickness (m)
L	Inductance (H)
$\Delta m$	Mass change (Kg)
Q	Quality factor
R	Resistance ( $\Omega$ )
Y	Admittance (Si)
Z	Impedance ( $\Omega$ )
$\lambda$	Wavelength (m)
$\rho$	Density (kg. m <sup>-3</sup> )
$\eta$	Bulk viscosity (Pa.s)
$\omega$	Angular frequency (Rad.s <sup>-1</sup> )
$\phi$	Phase (Rad)
$\epsilon_{22}$	Piezoelectric stress constant (A <sup>2</sup> . S <sup>4</sup> . Kg <sup>-1</sup> .m <sup>-3</sup> )
$e_{26}$	Permittivity (A.S.m <sup>-2</sup> )
$\bar{c}_{66}$	Quartz elastic constant (N.m <sup>-2</sup> )

## Subscripts

a	Anti-resonant
q	Quartz
r	Resonant
s	Series (resonant)

# Contents

<b>1</b>	<b>Introduction .....</b>	<b>6</b>
<b>2</b>	<b>Fundamentals and methods to model a QCM device.....</b>	<b>10</b>
2.1	QCM electrical equivalent circuit .....	10
2.2	Mass sensitivity of QCM .....	14
2.3	Quality factor.....	15
2.4	Quartz crystal oscillation modes .....	16
2.5	QCM200 device .....	19
2.6	Finite element analysis (FEM).....	21
2.6.1	FEM implementation using COMSOL .....	21
2.6.2	Device geometry .....	21
2.6.3	Boundary condition .....	22
2.6.4	Mesh optimization.....	22
<b>3</b>	<b>Results .....</b>	<b>26</b>
3.1	QCM200 electrical equivalent circuit simulation.....	26
3.2	The effect of the gold electrodes .....	28
3.3	The effect of change in radius of the device .....	30
3.3.1	The device in contact with air.....	30
3.3.2	The device in contact with water .....	31
3.4	Mechanical sensing .....	34
3.4.1	Bulk viscosity and density sensing.....	36
<b>4</b>	<b>Discussion .....</b>	<b>38</b>
4.1	Electrical equivalent model in MATLAB.....	38
4.2	FEM analysis model in COMSOL.....	38
<b>5</b>	<b>Conclusion and future work.....</b>	<b>41</b>
	<b>References .....</b>	<b>43</b>
	<b>List of figures .....</b>	<b>46</b>
	<b>List of Tables.....</b>	<b>48</b>
	<b>Example code .....</b>	<b>49</b>

# 1 Introduction

Sensors play an essential role in our daily life. Each electronic device includes at least one element which converts the input signal of one domain to an electrical output signal that can be quantified and translated to an action of the control system. There are numerous types of sensors in different applications, such as chemical sensors for the food industry[1]–[3], environmental compounds detection[4], [5], water treatment sensors[6], [7], and biomedical sensors[8], [9],[10], [11].

Increasing applications and demand for various markets lead to a more innovative and dynamic environment among scientists to create more efficient solutions. For detection systems like sensors, sensitivity, specificity, controllability, repeatability, environmental compatibility, and cost are important.

As sensors are energy converters, depending on the application, one sensing element might be more suitable compared to another. Furthermore, a combination of different sensor types like electrical, optical, acoustic, and thermal sensors provides multiple control over various parameters of a system.

Acoustic sensors are among the most promising devices due to their high sensitivity and specificity, low power consumption, and cost. These sensors are based on the piezoelectric properties of the material.

A piezoelectric material can produce polarization proportional to the applied mechanical stress and generate a mechanical deflection as a function of an applied voltage potential. A system that shows electromagnetic or mechanical resonant behavior is called a resonator. Piezoelectric resonators are considered mechanical resonators and are used to generate signals in specific frequencies. The resonant frequency is when the system oscillates with maximum amplitude. Similarly, anti-resonant frequency is where the system will oscillate with minimum amplitude. Although crystal resonators and crystal oscillators are the same in function, they are significantly different. Crystal resonators vibrate mechanically, while a crystal oscillator is an electric circuit that uses vibrating crystals to generate an electric signal with a specific frequency.

Resonators are named based on wave propagation types of surface acoustic wave (SAW), bulk acoustic waves (BAW), or acoustic plate mode (APM). In BAW devices, waves propagate through the bulk or volume of the piezoelectric material. The SAW wave propagation waves can be guided or unguided, and they travel across the surface of a

semi-infinite medium. In APM, waves are guided in plates or membranes whose thickness is comparable or thinner than their wavelength. These technologies are employed depending on the device's application and operation frequency.

Biosensors are important parts of medical diagnosis, biomolecular analysis, and food safety. For most clinical applications, biocompatibility, high sensitivity, high specificity, label-free, and disposable biosensors are desired. There are several techniques for fabrication bio resonators like quartz crystal microbalance (QCM), film bulk acoustic resonator (FBAR), Love wave acoustic sensor, microwave planar.[12]–[15]

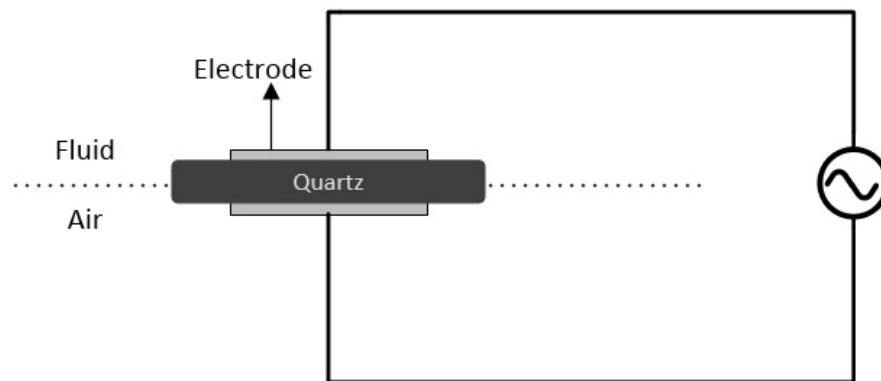


Figure 1: Schematic of QCM crystal

The QCM traces its origins back to the discovery of piezoelectricity of quartz in 1880 by Jacques and Pierre Curie[16]. QCM's working principle is based on the piezoelectric effect of quartz. Before 1959, there was not a significant move in the sensing application of quartz plates. In 1959, Sauerbrey proved that quartz oscillation frequency is dependent on surface mass[17]. He named it QCM, which focused on using quartz plate resonators as sensitive microbalances for thin films. He also proved that the oscillation frequency change is directly proportional to surface mass change. By saying that, the change in QCM frequency determines the mass adsorbed. Since then, this principle has been an integral part of transducers used in various fields such as material science, biosensors, environmental monitoring, etc. QCM is a BAW-based device consisting of a thin quartz disk with two gold electrodes on the top and the bottom of the quartz plate and an operating frequency of MHz.

QCM operates in the thickness-shear mode which two surfaces move in an anti-parallel fashion like in Figure 2

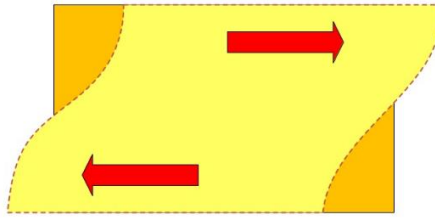


Figure 2: Thickness shear mode

The crystal plate must be cut to a specific orientation with respect to crystal axes so that acoustic waves propagate perpendicular to the crystal surface. There are AT and BT cuts concerning the angle of the cut. For AT-cut quartz, the cut angle is  $35^{\circ}15'$  from the Z-axis of the crystal. QCM is used in both dry and wet environments.

The electrodes are where we apply the electric potential. As a result of applying electric potential, acoustic waves are initiated inside the quartz. The resonant condition will occur if generated acoustic waves and reflected acoustic waves from the electrodes interfere constructively.

The resonant frequency depends on the device's material properties and geometry. The acoustic velocity of the acoustic waves depends on the medium they are passing through; thus, resonant frequency shifts as a result of a change in the medium surrounding the sensor. Plus, this leads to a virtual geometry change. Also, the resonant frequency will decrease upon adsorbing mass on the sensor's surface. Rudolf Bechemann demonstrated AT-cut quartz's frequency-temperature characteristics and temperature coefficient [18]. In AT-cut quartz, the temperature coefficient is independent of the dimension. This means that the change in dimension does not change the temperature behavior of the QCM. At room temperature ( $25^{\circ}\text{C}$ ), the temperature coefficient is very low, and resonant frequency dependence is zero [19]

QCM is used as a gas sensor for detecting different types of gases like  $\text{NH}_3$  and  $\text{HCL}$  [20]–[22]. Further application of QCM in liquid sensing is referred to in [22]–[25]. Viscosity and density are important parameters of the liquid, especially for biomedical samples. QCM offers decent signal strength, excellent temperature stability, and sensitivity. Furthermore, it is not expensive to manufacture, and it does not need harmful labels.

The final aim of this thesis is to investigate QCM behavior concerning changes in density and viscosity of the liquid water medium around it. We developed the QCM model to be

comparable to the real device used in laboratories. First, the system's electrical equivalent circuit (EEC) model is designed and investigated for the QCM in contact with air and water. Then real device simulation of the QCM is modeled and compared to the EEC model.

This thesis is structured as follows. This first chapter introduces the background, elaborates the working principle of the QCM, and reviews some previous works. Chapter two details the fundamental theories of device circuit modeling and describes the simulation and analysis. Chapter three demonstrates the results obtained from simulations, and chapter five includes discussions and conclusions followed by suggestions on future works. In appendix A, a small code example is added.

## 2 Fundamentals and methods to model a QCM device

In this chapter, some necessary concepts are addressed to understand the basis of the model. More details of the device are demonstrated, and two models are introduced. First is the ideal electrical equivalent model of a QCM, and the second is finite element analysis.

### 2.1 QCM electrical equivalent circuit

QCM as a resonator can store energy and transfer between two forms. The resonant frequency is the frequency where this transfer is more efficient. There is a tendency to model mechanical devices in their equivalent circuit model to investigate their behavior. There are many different circuit models that describe the electrical behavior of a resonator[27]. In 1914, Butterworth introduced the first electrical equivalent circuit to represent a resonator [28]. Some years later, in 1925, K.S. Van Dyke discovered that the same circuit also characterized the impedance behavior of a piezoelectric resonator[29]. Then in 1930, W.P. Mason extended the use of electromechanical conversion by introducing acoustic transmission lines, mechanical ports, and piezoelectric transformers[30]. In 1991 Martin and Granstaff modified the QCM model considering mass and liquid load[31]. From these studies, Butterworth-Van Dyke's (BVD) model is introduced, which is a general electrical model of resonators[32]. The resonator is modeled by a circuit which capacitance  $C_0$  is parallel to an acoustic arm. Other emotional arms that correspond to resonance are parallel to the acoustic arm, shown in Figure 3. Higher-order harmonics are negligible when the frequency of interest is the resonant frequency.

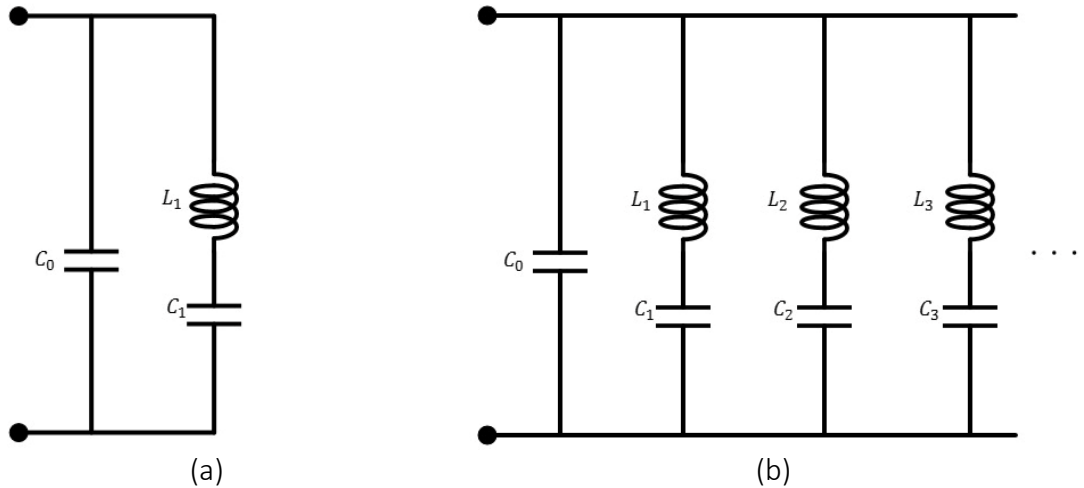


Figure 3:(a) Single resonant BVD, (b) Multi resonant BVD each motional arm corresponds to a resonance[32]

The QCM as a resonator can be modeled using the BVD circuit. For the QCM in contact with the fluid, the BVD circuit is like Figure 4

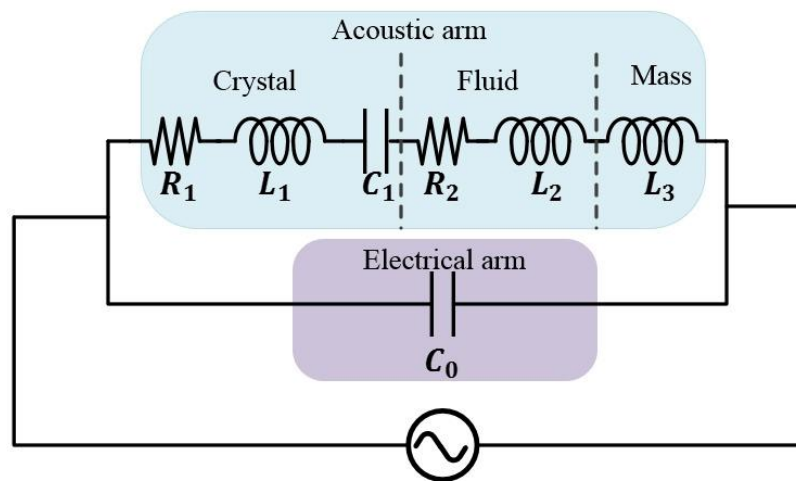


Figure 4: Butterworth–van-Dyke circuit representation of QCM (BVD)[31]

$C_0$  capacitance is the static capacitances of the crystal's electrodes

$R_1$  resistor is the dissipation of oscillation energy in the crystal and the surrounding medium

$L_1$  inductor is the inertial mass of the bare crystal

$C_1$  capacitor is the stiffness of the crystal and the stored energy in the oscillation.

$R_2$  resistor is the real part of the surface impedance (dissipation due to fluid viscosity and density)

$L_2$  inductor is liquid mass loading

$L_3$  inductor is added mass

In the modified model, Martin and Granstaff characterized all the circuit parameters according to the below equations from which we can realize that parameters values are dependent on material characteristics and dimensions of the quartz crystal[31]:

$$C_0 = \frac{\epsilon_{22}A}{h} \quad (2-1)$$

$$C_1 = \frac{8 \cdot e_{26}^2 A}{(N \cdot \pi)^2 \cdot \bar{c}_{66} \cdot h} \quad (2-2)$$

$$L_1 = \frac{1}{\omega_s^2 \cdot C_1} \quad (2-3)$$

$$R_1 = \frac{\eta_{66}}{\bar{c}_{66} \cdot C_1} \quad (2-4)$$

$$L_2 = \frac{2 \cdot \omega_s \cdot L_1 \cdot \rho_s}{N \cdot \pi} \left( \frac{1}{\bar{c}_{66} \cdot \rho_s} \right)^{1/2} \quad (2-5)$$

$$L_3 = \frac{\omega_s \cdot L_1}{N \cdot \pi} \left( \frac{2 \cdot \rho \cdot \eta}{\bar{c}_{66} \cdot \omega \cdot \rho_s} \right)^{1/2} \quad (2-6)$$

From the combination of both series and parallel LC circuits in the BVD equivalent circuit, resonant and anti-resonate behavior of the QCM is described. By knowing that impedance is the opposition that the circuit shows against the current flow, the input impedance of the simplified circuit is like equation (2-7):

$$Z(\omega) = \frac{j \left( \omega L_1 - \frac{1}{\omega C_1} \right)}{1 - \omega^2 C_0 L_1 + C_0 / C_1} \quad (2-7)$$

In resonant frequency,  $Z(\omega)$  is minimum and reactance of the motional arm equal to zero, which means the only limitation for current flow is  $R_x$  and  $R_1$ . The admittance  $Y$  is the reciprocal of impedance and the measure of how easily an electrical current (i.e., the flow of charge) can pass through a material.

$$Y = i\omega C_0 + \frac{1}{Z(\omega)} \quad (2-8)$$

conductance  $G(\omega)$  is the reciprocal of the total resistance ( $1/R$ ) or real part of the admittance

$$G(\omega) = \frac{R}{R^2 + (\omega L - 1/\omega C)^2} \quad (2-9)$$

Where R is the total resistance (dissipation), L is the total inductance and reflects the stored kinetic energy, and C is the capacitance or stored potential energy.

$$R = R_1 + R_2 \quad (2-10)$$

$$L = L_1 + L_2 + L_3 \quad (2-11)$$

$$C = C_1 \quad (2-12)$$

As described above, the resonant frequency is where the  $Z(\omega)$  is minimum or  $G(\omega)$  is maximum. From equations, we extract that maximum conductance happens when  $L_1$  and  $C_1$  are canceling each other, so resonant frequency is obtained.

$$\omega_r = \frac{1}{\sqrt{L_1 C_1}} \quad (2-13)$$

anti-resonant frequency is where  $Z(\omega)$  is maximum, and reactance of the loop formed by the motional arm and electrostatic branch equals zero. anti-resonant frequency is achieved as following

$$\omega_a = \sqrt{\frac{C_1 + C_0}{L_1 C_1 C_0}} = \omega_r \cdot \sqrt{1 + \frac{C_1}{C_0}} \quad (2-14)$$

At resonant frequency where  $\omega L = \frac{1}{\omega C}$ , the normalized conductance is defined as

$$\bar{G}(\omega) = RG(\omega) = \frac{R^2}{R^2 + (\omega L - 1/\omega C)^2} \quad (2-15)$$

Itoh A and Ichihashi M, 2008 illustrated that at a critical frequency ( $\omega^*$ ), the normalized conductance of the quartz crystal is not affected by the viscosity and density of the surrounding media[33].

$$\bar{G}(\omega^*) = \frac{R_1^2}{R_1^2 + (\omega^* L_1 - 1/\omega^* C_1)^2} \quad (2-16)$$

$$\bar{G}(\omega^*) = \frac{(R_1 + R_2)^2}{(R_1 + R_2)^2 + (\omega^*(L_1 + L_2) - 1/\omega^*C_1)^2} \quad (2-17)$$

At  $(\omega^*)$  equations (2-16) and (2-17) are equal, which result in

$$R_2 = \omega L_2 \quad (2-18)$$

so, at  $\bar{G} = 0.5$ , the fluid resistance and inductance cancel each other.

## 2.2 Mass sensitivity of QCM

Quartz crystal resonators (QCR) are sensitive to mass absorption on their surface. In 1959 Sauerbrey demonstrated that the frequency change of the oscillating quartz is linearly related to the mass change on its surface[31]

$$\Delta m = -C \times 1/n \times \Delta f \quad (2-19)$$

According to the above, the resonant frequency of the QCM will decrease upon mass absorption. Thus, the mass absorbed by the device can be measured from the frequency shift. This frequency shift is calculated based on the weak coupling of shear waves into the liquid. However, according to previous sections, this frequency shift is also affected by the surrounding medium. The dependence of the resonant frequency shift on the area density of the adsorbed mass ( $\rho_m$ ) and the density ( $\rho$ ) and viscosity ( $\eta$ ) of the surrounding fluid is demonstrated in the below equation.

$$\Delta f_c \approx \frac{2f_c^2}{N\sqrt{\bar{C}_{66}\rho_q}} \left[ \rho_m + \left( \frac{\rho\eta}{4\pi f_c} \right)^{1/2} \right] \quad (2-20)$$

Where  $f_c$  is the resonance frequency of the Nth mode,  $\bar{C}_{66}$  is the piezoelectrically stiffened quartz elastic constant, and  $\rho_q$  is the crystal density. According to the above, it is impossible to distinguish the portion of mass absorption effect from the fluid density and viscosity effect in frequency change. Therefore, the center frequency cannot be used reliably to determine mass adsorption when it is concurrent with fluid viscosity and density variations. This thesis aims to measure the effect of viscosity and density change on center frequency change; therefore, mass absorption is not considered in evaluations.

## 2.3 Quality factor

One of the most critical parameters designing a resonator is the device's quality (Q) factor. Real resonators always have losses that should be considered in the design despite an ideal resonator that never loses energy and vibrates with the same intensity even in the absence of the trigger force. In the BVD model, the resistors represent the losses which are shown in Figure 5

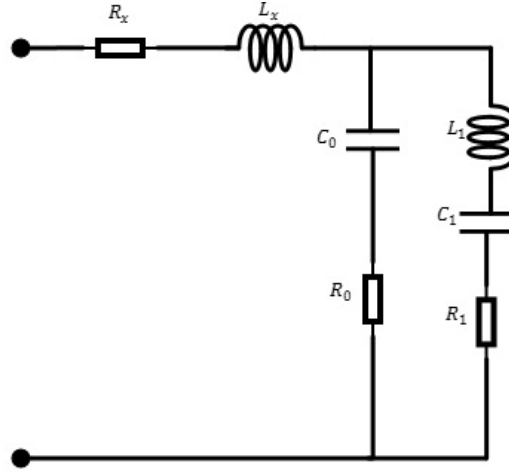


Figure 5: The modified BVD (mBVD) considering losses

The Q factor is the rate of energy loss by the resonator. To rephrase, the Q factor is the ratio of the energy stored in the oscillating resonator to the energy dissipation per cycle by the damping process [34].

$$Q = 2\pi \times \left( \frac{\text{Energy stored}}{\text{energy dissipated per cycle}} \right) = 2\pi f_r \times \left( \frac{\text{Energy stored}}{\text{power loss.}} \right) \quad (2-21)$$

For simplified BVD, the Q factor is calculated from the steepness of the phase curves at the resonant and anti-resonant frequency, and  $\varphi$  is the phase angle of the impedance.

$$Q_{r,a} = \frac{f_{r,a}}{2} \left( \frac{d\varphi(Z)}{df} \right) \Big|_{f_{r,a}} \quad (2-22)$$

the  $Z(\omega)$  of the BVD circuit is:

$$Z(\omega) = j\omega L_x + R_x + \left[ \frac{1}{R_0 + \frac{1}{j\omega C_0}} + \frac{1}{R_1 + j\left(\omega L_1 - \frac{1}{\omega C_1}\right)} \right]^{-1} \quad (2-23)$$

Where  $R_x$  is the resistance of the metal electrodes connecting the device and  $L_x$  is associated with device layout on the wafer or measurement configuration.

The quality factors at series and parallel resonances are

$$Q_r = -\frac{1}{2} \omega_r \left. \frac{\partial \varphi}{\partial \omega} \right|_{\omega=\omega_r} \quad (2-24)$$

And

$$Q_a = +\frac{1}{2} \omega_a \left. \frac{\partial \varphi}{\partial \omega} \right|_{\omega=\omega_a} \quad (2-25)$$

From mBVD, an approximation of the Q factor in resonance and anti-resonance frequency is achieved according to the below equations.

$$Q_r \approx \frac{\omega_r L_1}{R_x + R_1} \quad (2-26)$$

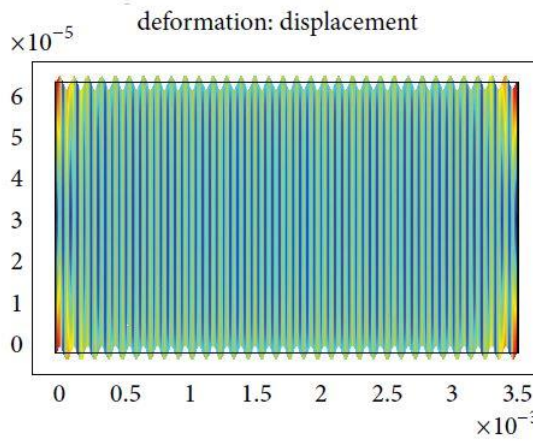
And

$$Q_a \approx \frac{\omega_a L_1}{R_0 + R_1} \quad (2-27)$$

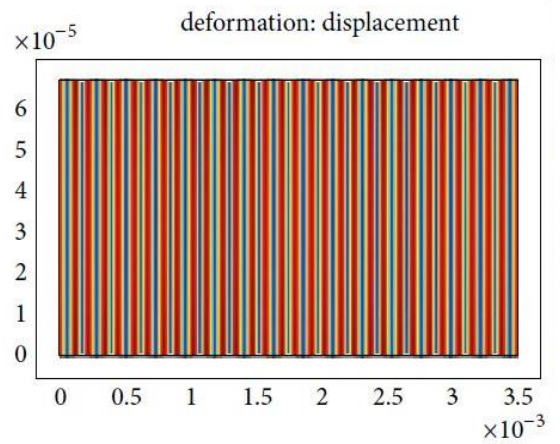
From equations (2-26) and (2-27), the main parameters to the resonant Q value are  $R_x$  and  $R_1$ , while for anti-resonant frequency,  $R_0$  and  $R_1$  are the main contributors. In resonant frequency,  $R_x$  is present due to the high currents associated with the series resonant.

## 2.4 Quartz crystal oscillation modes

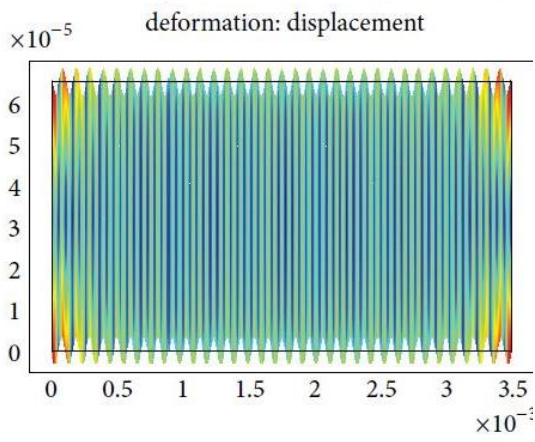
As described in section one, quartz is an anisotropic piezoelectric material whose crystal oscillation is affected by different cutting angles or temperature changes. There are natural vibrations associated with a quartz crystal which differs from the vibrations triggered by the applied voltage on the electrodes. Zi-Gui Huang and Zheng-Yu Chen [35] have analyzed thin AT-cut quartz in the frequency range of 25 MHz-27MHz, which results in sixteen natural harmonics and seven excited harmonics. They introduced four basic modes of flexural, thickness-shear, coupled mode of the flexural and thickness-shear, and the extension mode for a two-dimensional thin AT-cut quartz plate. They divided these modes into two types: symmetric modes that cannot be excited and antisymmetric modes that can be excited. The shape of each mode is shown in below Figure 6 (a-J)



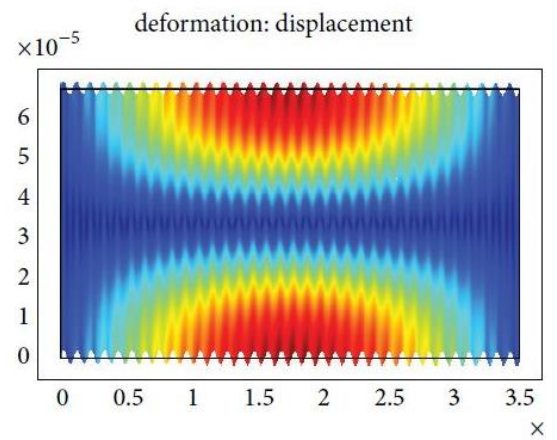
(a) Flexural mode-symmetric resonance



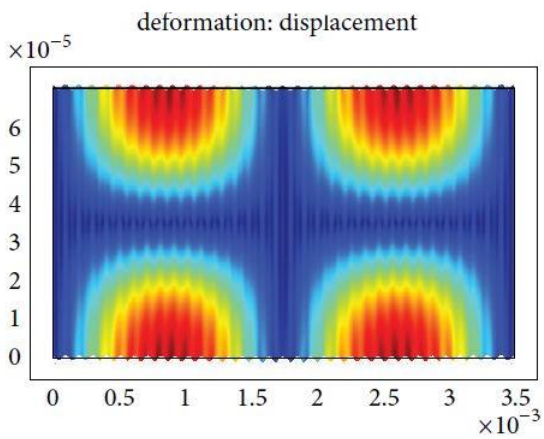
(b) Extension mode-symmetric resonance



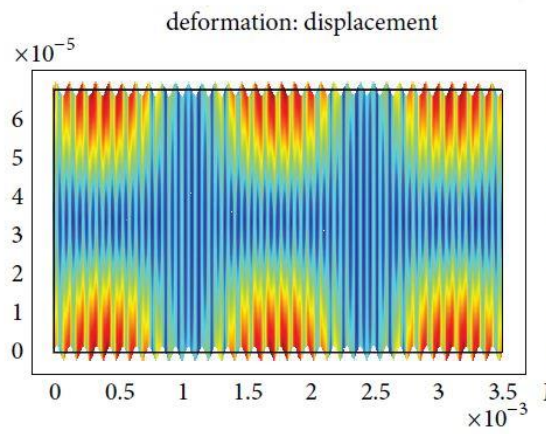
(c) Flexural mode-symmetric resonance



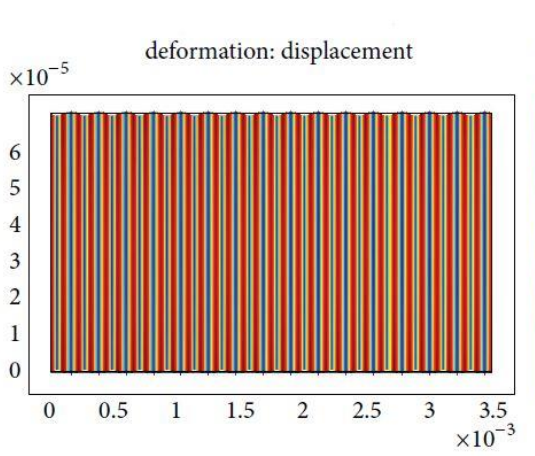
(d) Thickness shear mode-antisymmetric



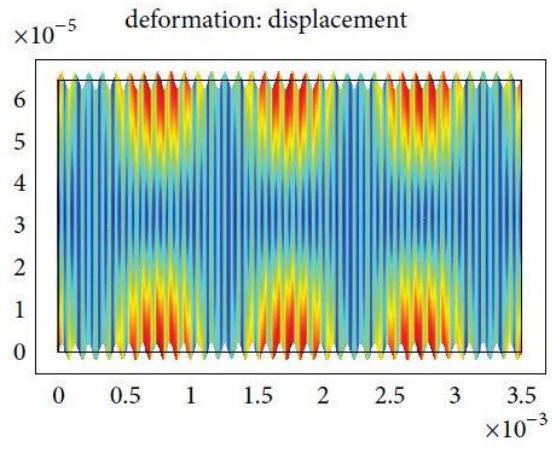
(e) coupled mode-symmetric resonance



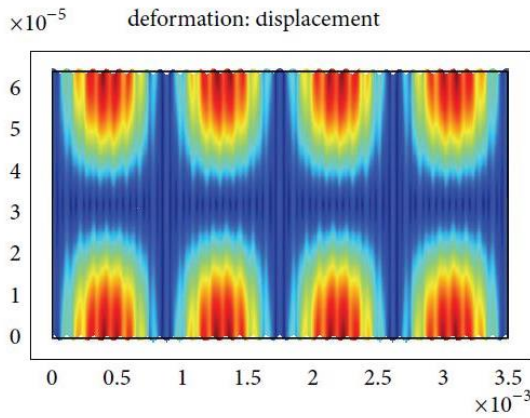
(f) Coupled mode-antisymmetric resonance



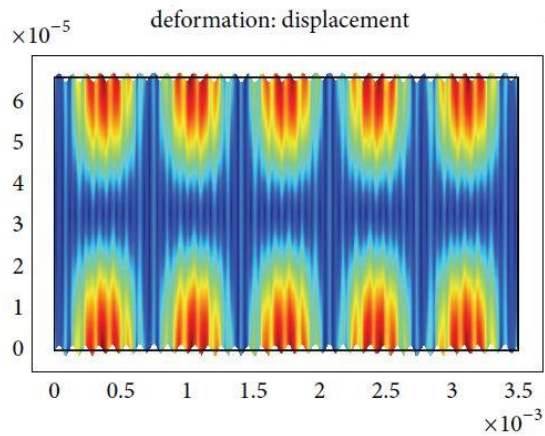
(g) Extension mode-symmetric resonance



(h) Coupled mode-antisymmetric resonance



(i) Coupled mode-symmetric resonance



(j) Coupled mode-antisymmetric resonance

Figure 6: Mode shapes[35]

QCM operating mode is based on thickness-shear mode, which can be excited by an external voltage. As a result of applying voltage on top of the QCM, a wave transfers in the thickness direction that is called thickness-shear waves. However, some radial waves are also generated, known as thickness twist. The resonant frequency results from passing the thickness-shear waves through the crystal while the twist waves are in harmonic waves, which are not desired and may deteriorate the accuracy of resonant frequency measurement; thus, it is important to eliminate such unwanted frequencies.

## 2.5 QCM200 device

The QCM device which is modeled in this thesis is the QCM200 system. The instrument includes a controller, crystal oscillator electronics, crystal holder, and three quartz crystals. The information in this section is obtained from the QCM200 user manual.



Figure 7: Complete QCM setup consisting of QCM200 digital controller, QCM25 crystal oscillator, crystal holder, and three quartz crystal sensors

The sensor is a QCM25 crystal oscillator, AT-cut quartz sandwiched in gold electrodes on the top and bottom of the quartz plate. The sensor is placed in a holder which consists of orings, contact springs, retainer ring, and retainer cover.

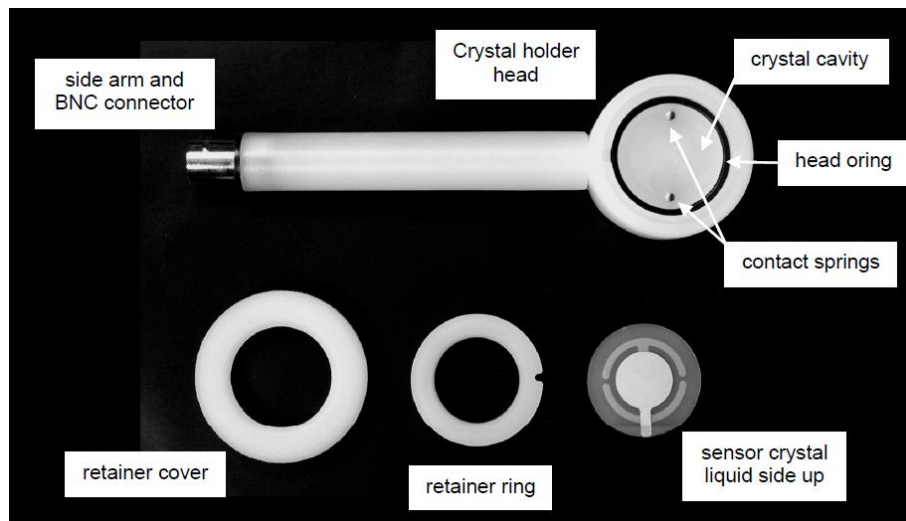
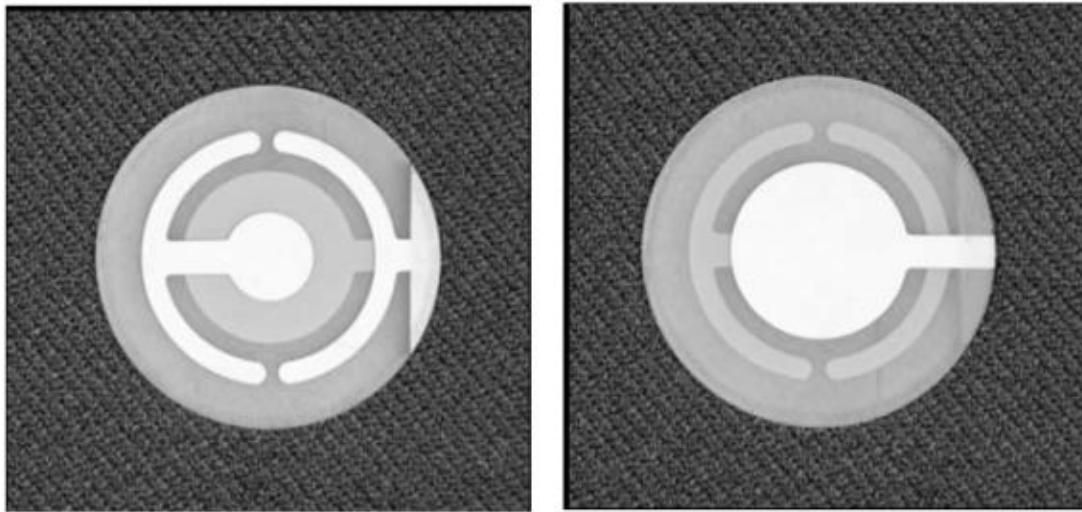


Figure 8: Crystal holder components

The device's operating frequency is 5MHz with respective dimensions 269.875x50.8x177.8 mm<sup>3</sup> (WHD), and the total weight of the device is 907,18 gr.

The contact surface has two separate circuits and a smaller electrode pad, while the liquid surface has a larger electrode pad. The liquid surface can be in direct contact with gas and liquid.



(a)

(b)

Figure 9:(a) Contact surface of QCM (b) Liquid surface of QCM

The BVD circuit parameters for QCM200 with a diameter of 1" (25,4 mm) in contact with air and DI water are according to Table 1 :

Table 1: BVD circuit parameters of QCM200

	$R_1(\Omega)$	$L_1(\text{mH})$	$C_1(\text{fF})$	$R_2(\Omega)$	$L_2(\mu\text{H})$
Air	10	30	33	0	0
DI water	10	30	33	390	12.8

For this device, the parasitic capacitance,  $C_0$ , which represents the sum of the static capacitances of the crystal's electrodes, holder, and connector capacitance, is 20pF. Unfortunately,  $C_0$  cannot be ignored in QCM and should be canceled at the operation time; otherwise, the measurements are inaccurate. Several methods of cancellation for  $C_0$  are introduced in the manual of the device.

Accordingly, a MATLAB model of an RLC circuit is developed to investigate the ideal QCM200 behavior in contact with air and water.

## 2.6 Finite element analysis (FEM)

FEM is a widely used method to solve differential equations numerically. Using FEM make it possible to predict the device reactions toward vibrations, heat, real-world forces, fluid flow, and other physical parameters. The merit of using FEM is the possibility of considering all the effects of mentioned physical parameters simultaneously. Furthermore, it divides a complex system into smaller subsystems called finite elements, which results in simpler analysis and thus minimum errors. Then these finite elements are assembled and form a large system that models the device. There are several commercially available software forms to perform FEM, namely ANSYS, COMSOL, Convertor, etc. In this thesis, a 3D model of the QCM200 device is implemented in COMSOL 5.6.

### 2.6.1 FEM implementation using COMSOL

The design is modeled according to the following steps; more illustration is provided for some of the steps:

- 1- Defining the structure and choosing piezoelectricity as structural mechanics, which is a combination of solid mechanics and electrostatic physics.
- 2- Building up the geometry of the QCM200 in contact with liquid
- 3- Choosing the material
- 4- Setting the initial condition of the system and boundary constraints
- 5- Meshing the structure
- 6- Choosing the frequency domain as the type of study
- 7- Solving equations are applied

### 2.6.2 Device geometry

The QCM device in contact with liquid is modeled as a cylinder of AT-cut quartz with two thin gold electrodes on top and bottom of the device. Both electrodes are defined as a linear elastic material. The top electrode is where the AC voltage is applied while the bottom electrode is grounded. Another cylinder placed on top of the electrode represents the liquid layer, which is water in this study. A perfectly matched layer (PML) is considered on top of the water interface as an artificial absorbing layer of waves which helps avoid acoustic waves reflecting. Figure 10 shows the 3d structure of the geometry.

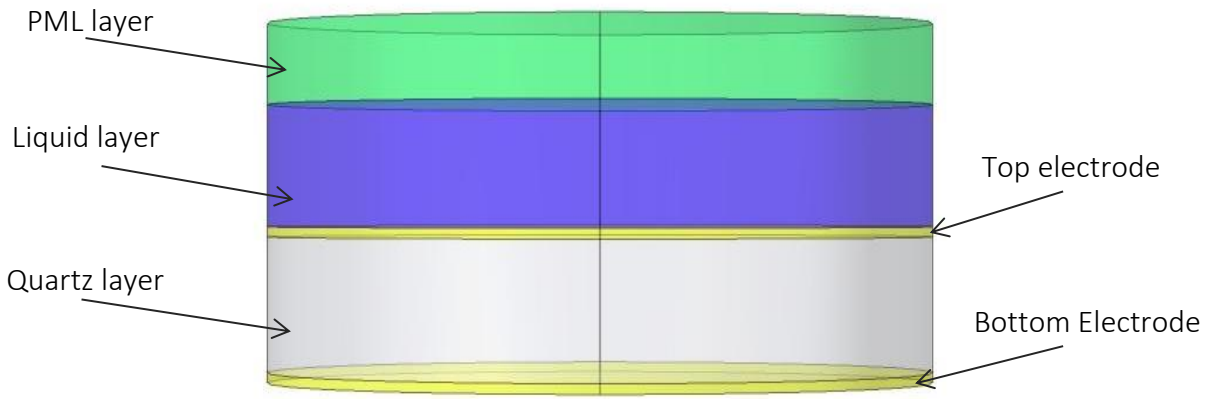


Figure 10: Model geometry

The water and PML layer thickness are arbitrary numbers representing the semi-infinite condition; however, these values should be small to achieve fine optimization. Notably, the PML layer should be thick enough to absorb all the waves transmitted through the liquid layer. Plus, the liquid layer thickness should be bigger than the penetration depth of the shear component[36]. Consequently, the water and PML layer thickness are  $1\mu\text{m}$  and  $3\mu\text{m}$ , respectively.

### 2.6.3 Boundary condition

In order to resemble the real device working condition, the boundary conditions of each domain are defined separately. The electrodes material is gold, and they are considered as linear elastic material. The electric potential is applied to the electrodes while the bottom electrode is grounded. The quartz layer is defined as piezoelectric material with which all boundaries are free. Both PML and liquid domains are modeled using pressure acoustic frequency module. All the boundaries for the PML layer are set as sound hard boundary (wall). This represents the absorption of the acoustic wave in the PML layer (zero velocity). However, for the liquid domain, the side walls are defined as the sound soft boundary where the acoustic pressure vanishes.

### 2.6.4 Mesh optimization

Another important parameter for the optimized model is the meshing of the layers. The minimum frequency of the acoustic wave for QCM200 is  $\lambda_0 = 668\mu\text{m}$ . The meshing characterization of the piezoelectric layer should be in a way that the resonant frequency of the device does not change with respect to a higher number of elements, and the

saturation is reached. This is achieved at  $\lambda_0/8$  for the piezoelectric layer. To ensure that the mesh is optimized, we set the number of elements based on  $\lambda_0/10$ .

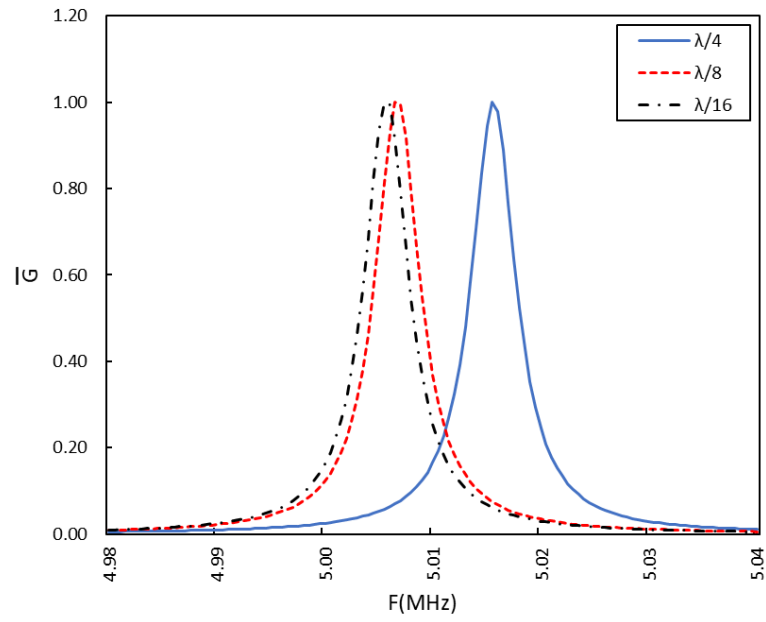
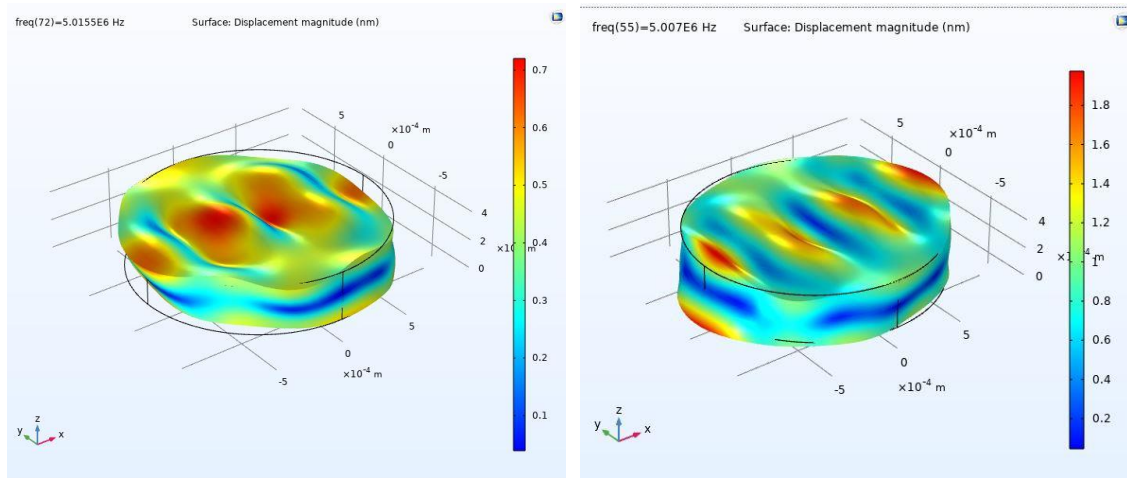
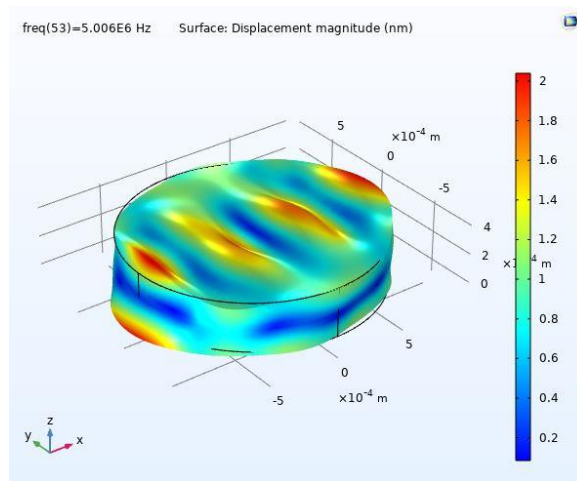


Figure 11: Mesh optimization based on wavelength



(a)

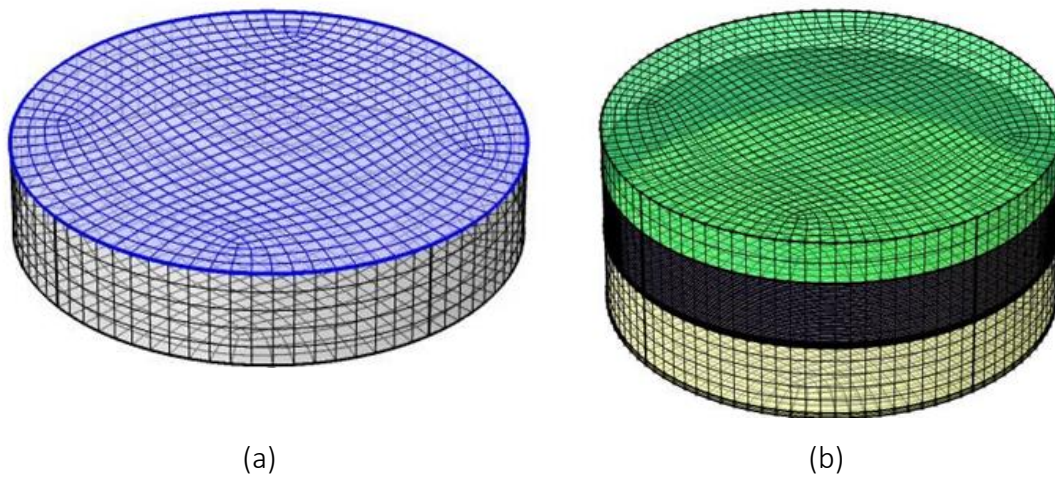
(b)



(c)

Figure 12: QCM displacement response to mesh optimization (a)  $\lambda/4$ , (b)  $\lambda/8$ , (c)  $\lambda/16$

The electrodes and PML layer follow the same meshing structure. A very fine mesh is needed for the liquid layer, so the number of elements is 40. The different sweeping mode does not change the meshing efficiency, so the quadrilateral is used. The efficiency of the computation is highly dependent on several elements; thus, it is important to consider a reasonable number of elements. The finer the mesh, the longer the simulations. The meshing structures are shown in Figure 13:



(a)

(b)

Figure 13: (a) Meshing structure of the piezoelectric layer (b) Meshing structure of the model.



### 3 Results

In this chapter, the results of simulations based on the methods described in the previous chapter are illustrated. The results are categorized in different sections and are obtained from MATLAB and COMSOL.

#### 3.1 QCM200 electrical equivalent circuit simulation

To assess the electrical sensing of the QCM, the BVD circuit of the QCM200 is modeled in MATLAB with the given values for circuit parameters in chapter two. The behavior of the system is further investigated by plotting impedance, normalized conductance ( $\bar{G}$ ), normalized susceptance (B), and impedance phase ( $\phi$ ) versus frequency (F).

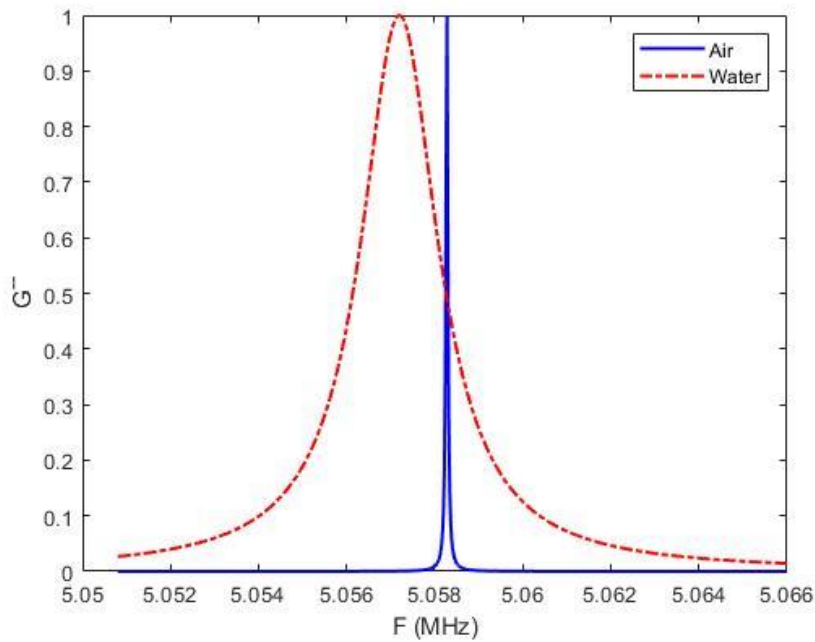


Figure 14: Normalized conductance versus frequency (MATLAB results)

The conductance figure shows the frequency shift of 1kHz upon adding motional arm  $R_2$  and  $L_2$ , representing the water layer. Besides this, the response is broader due to the higher value of the resistance (dissipation). The susceptance graphs represent the phase of the admittance, which are shown in Figure 15

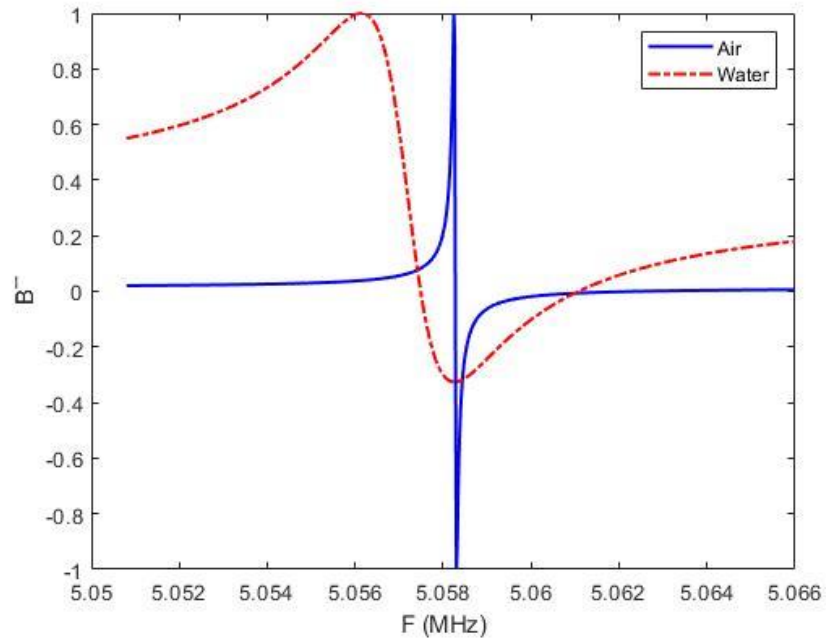


Figure 15: Susceptance versus frequency (MATLAB results)

From the impedance plot, we can extract both resonant and anti-resonant frequency of the device in contact with air and water.

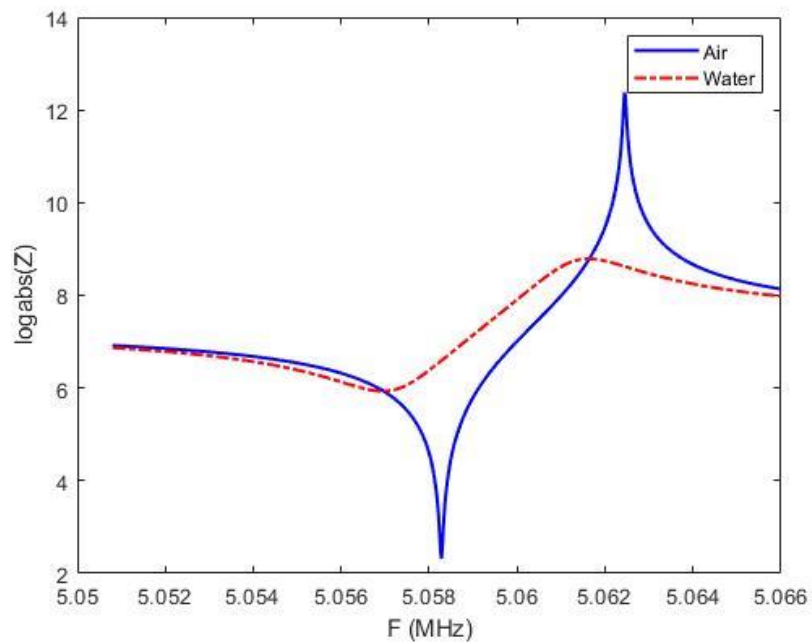


Figure 16: Impedance versus frequency (MATLAB results)

Based on the above, the resonant frequency ( $f_r$ ) and anti-resonant frequency ( $f_a$ ) of the device in contact with air are 5.058 MHz and 5.062 MHz, respectively. For the device in contact with water, the frequency shifts 1000 Hz, which results in resonant frequency 5.057 MHz and anti-resonant frequency of 5.061 MHz.

The quality factors ( $Q_r$ ) of the device in contact with air and water are extracted from phase and derivative of phase plot according to the equation 2-26, which is 94247 and 2357, respectively. The Q factor decrease in contact with water sets clear that the performance when working in liquid is determined to a large extent by the liquid losses.

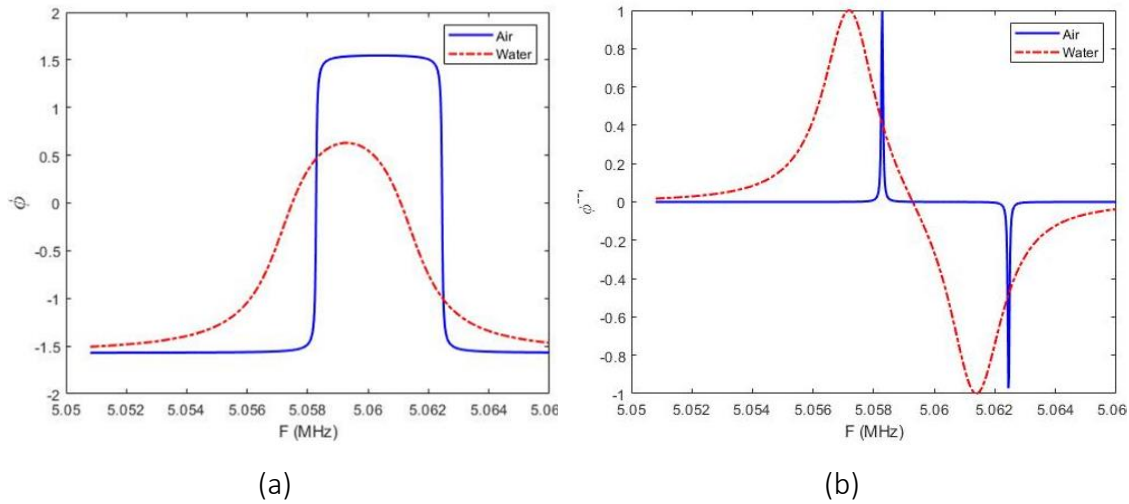


Figure 17: (a) Impedance phase. (b) derivative of impedance phase (MATLAB results)

### 3.2 The effect of the gold electrodes

As mentioned in the previous chapter, QCM is a mass-sensitive sensor that can detect mass changes in the range of nanograms. According to the Sauerbrey equation(2-19), it is expected to see a shift in the device's resonant frequency when a thin layer of the gold electrode is added on the top and bottom of the quartz layer. To find out the effect of the gold electrode on the resonant frequency, first, the device is modeled without gold electrodes, and then frequency shift is measured after adding the electrodes. To have an efficient simulation, the radius of the QCM device is considered  $835\mu\text{m}$ , and the thickness of the gold electrode is  $0.5\mu\text{m}$ . The results are extracted from COMSOL and shown in Figure 18.

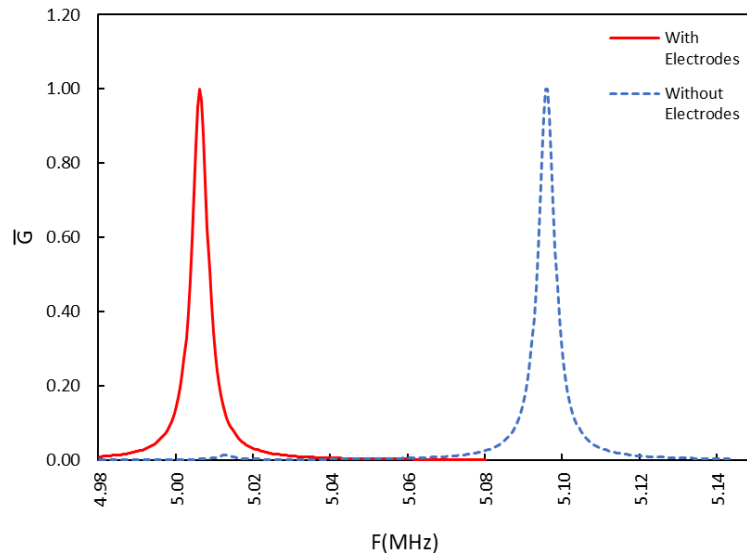
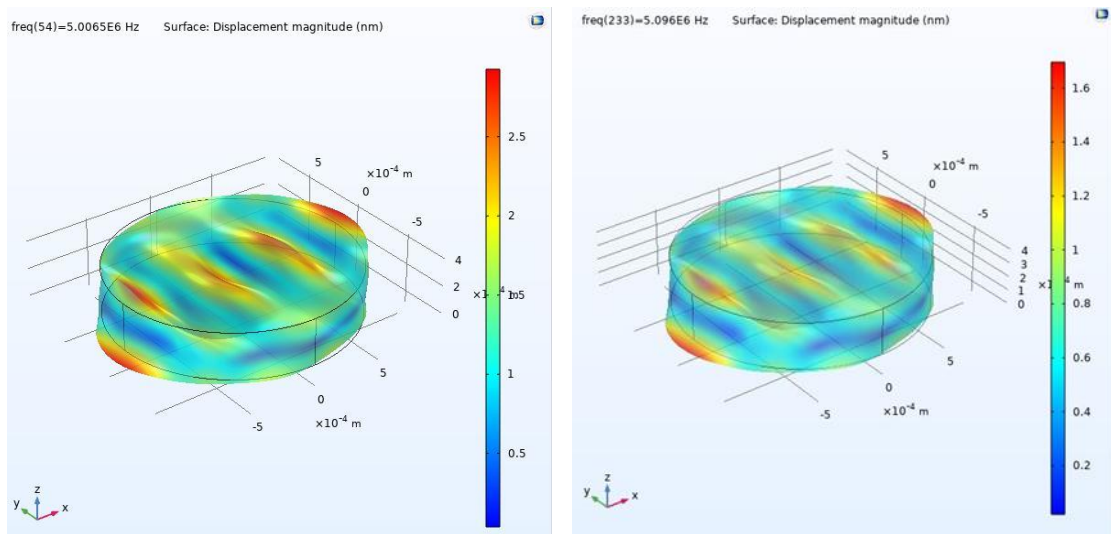


Figure 18: QCM response with electrode & without electrode (COMSOL results)

From the above response, we can see the resonant frequency shifts from 5.096 MHz to 5.0065 MHz, which shows an 89.5 KHz shift of resonant frequency. The displacement figures of the device are according to the below.



(a)

(b)

Figure 19: Surface displacement magnitude of the QCM (a) with the electrodes (b) without electrodes (COMSOL results) (COMSOL results)

Figure 19(a) shows that the surface displacement magnitude is increased by adding electrodes. The thickness-shear nature of the QCM in resonant frequency is obvious in the electrical potential cut-out figures.

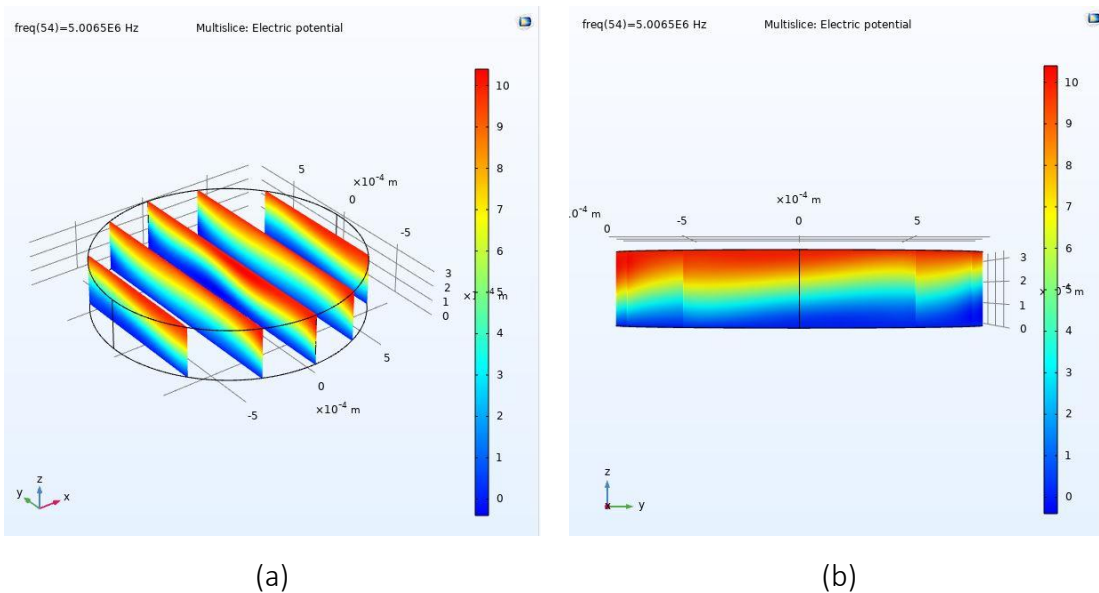


Figure 20: Electric potential of the QCM with electrodes at resonant frequency (a) 3D view cut out (b) 2D view cut out (COMSOL results)

### 3.3 The effect of change in radius of the device

Due to simulation time and hardware limits, we cannot model the geometry of the real device (sensor radius equal to 3500 $\mu$ m). As mentioned in previous sections, the device geometry affects the device's operating frequency. Several simulations are performed to determine the effect of area on frequency change, which are described in the below subsections.

#### 3.3.1 The device in contact with air

For the device in contact with air, the effect of change in the radius of the sensor is investigated. To find the optimal radius with minimal error due to changes in device geometry, the device is modeled in three different radii of 535 $\mu$ m, 835 $\mu$ m, and 1035 $\mu$ m. The results represent the resonant frequency of all three devices with electrodes and in contact with air.

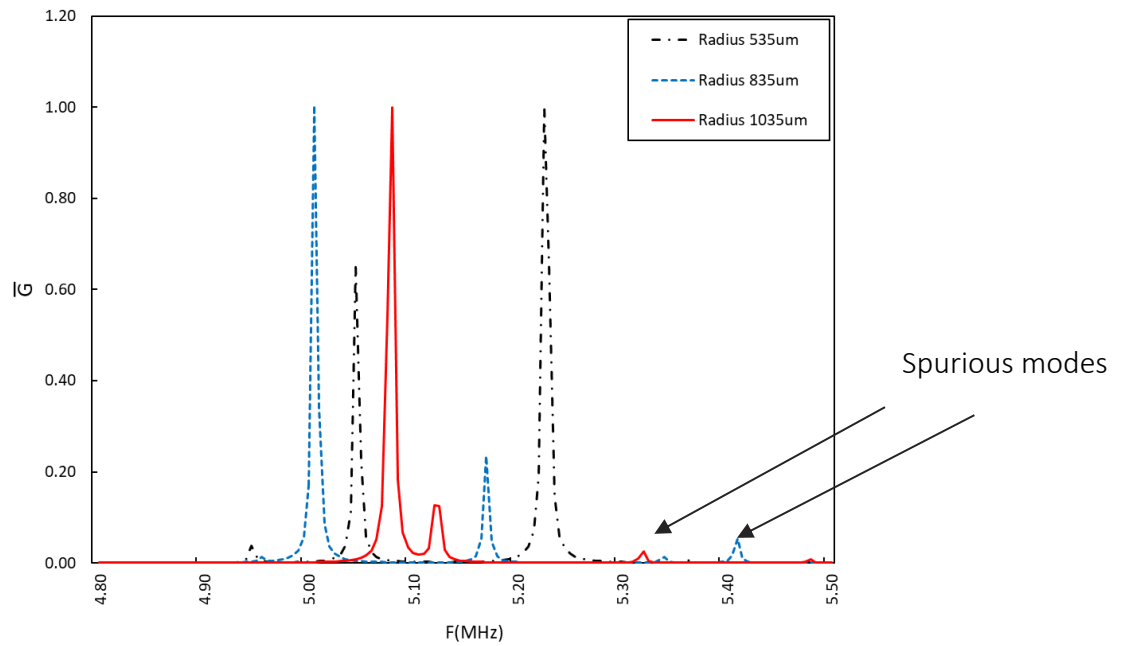


Figure 21: The effect of change in radius on the resonant frequency (COMSOL results) According to the above graph, the optimal radius of the QCM in contact with air is 835 $\mu\text{m}$  which gives the resonant frequency of 5.09MHz. The spurious response appears from edge reflections (ripples in Figure 21).

Another simulation in MATLAB is performed to compare the resonant frequency of the optimum radius of 835 $\mu\text{m}$  and the real device with a radius of 3500 $\mu\text{m}$ . The values of the BVD circuit are calculated based on the characterization equations in chapter two and are presented in Table 2:

Table 2: Values of BVD parameters for the device in contact with air

Radius( $\mu\text{m}$ )	$R_1(\Omega)$	$L_1(\text{mH})$	$C_1(\text{fF})$	$R_2(\Omega)$	$L_2(\mu\text{H})$	F(Hz)
3500	10	33	30	0	0	5057300
835	187	581	1.7	0	0	5064160

The resonant frequency of the BVD circuit for the device with the radius of 3500 $\mu\text{m}$  and 835 $\mu\text{m}$  is 5.057 MHz and 5.064 MHz, respectively. Thus, the effect of change in the area of the device 6.8 KHz positive shift of the resonant frequency.

### 3.3.2 The device in contact with water

When the device is in contact with water, further to the change in geometry, the loading effect of the water layer plus viscosity and density of the liquid affects the operating

frequency of the device. To investigate these effects more, the BVD circuit of the device is modeled with the radius of 835 $\mu\text{m}$  and 3500 $\mu\text{m}$ . The values of  $R_2$  and  $L_2$  are calculated from the characteristics equations mentioned in chapter two, then the corresponding center frequency (F) results from MATLAB simulation.

Table 3: Values of BVD parameters in contact with water (a) device radius 3500 $\mu\text{m}$  (b) device radius 835 $\mu\text{m}$

(a)

Radius( $\mu\text{m}$ )	T( $^{\circ}\text{C}$ )	$\eta_w$ (mPa. s)	$\rho_w$ (kg. m $^{-3}$ )	$R_2$ ( $\Omega$ )	$L_2$ ( $\mu\text{H}$ )	F(Hz)
3500	20	1.0016	998.20	302.53	9.52	5056560
	25	0.8880	997.00	285.03	8.97	5056620
	30	0.7972	995.61	269.55	8.48	5056650
	35	0.7191	994.0	255.8	8.05	5056680
	40	0.6527	992.22	243.48	7.66	5056720

(b)

Radius( $\mu\text{m}$ )	T( $^{\circ}\text{C}$ )	$\eta_w$ (mPa. s)	$\rho_w$ (kg. m $^{-3}$ )	$R_2$ ( $\Omega$ )	$L_2$ ( $\mu\text{H}$ )	F(Hz)
835	20	1.0016	998.20	5315.38	167.29	5063440
	25	0.8880	997.00	5007.50	157.60	5063480
	30	0.7972	995.61	4735.92	149.05	5063520
	35	0.7191	994.00	4494.34	141.45	5063540
	40	0.6527	992.22	4277.94	134.64	5063580

To illustrate more the obtained results, the graph of the frequency shift with respect to the temperature increase is shown in Figure 22. The obtained results are compared with the experimental data achieved from the QCM200 [37].

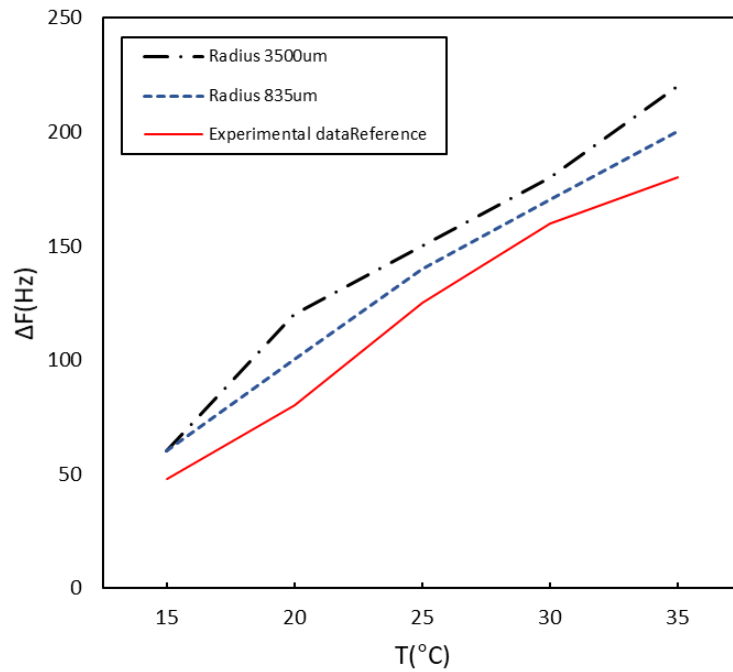


Figure 22: Frequency change of the QCM devices with radius 835 $\mu\text{m}$ ,3500 $\mu\text{m}$  obtained from BVD in MATLAB, and QCM200 reference data

From the above graph, we can see that the simulations of the BVD circuits follow the experimental data obtained from the real device with small deviations.

Another FEM analysis is performed to investigate the resonant behavior of the QCM in contact with water. So, the QCM was modeled with both radius 835 $\mu\text{m}$  and 1035 $\mu\text{m}$ . The results are shown in Figure 23

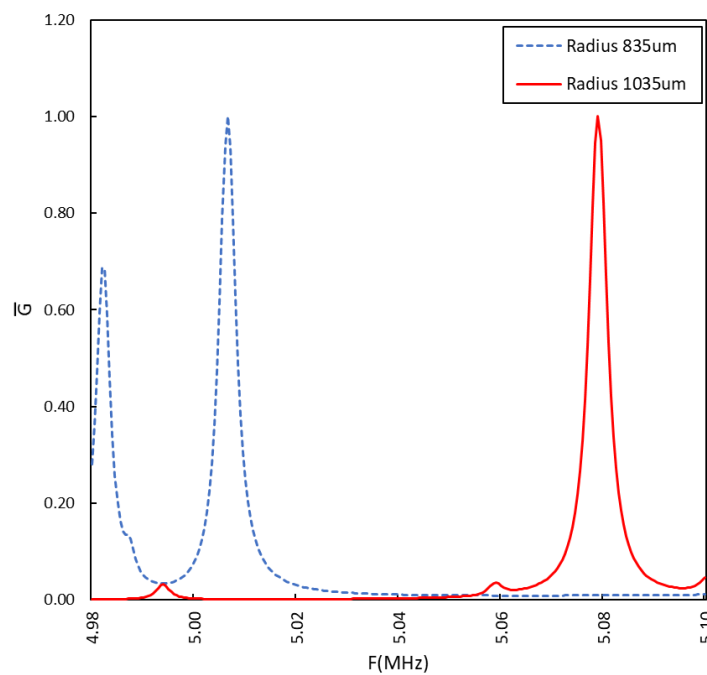


Figure 23: QCM response in contact with water (COMSOL results)

From the above figure, we can see that the response for the QCM with a radius of 835 $\mu\text{m}$  is too close to another peak which affects the quality of the resonant frequency, while for the device with the radius of 1035 $\mu\text{m}$ , the signal is strong and reliable. So, for investigating the device behavior in water, the optimum radius for FEM analysis is considered 1035 $\mu\text{m}$ .

### 3.4 Mechanical sensing

The simulated results using the device with gold electrodes on top and bottom, where density, shear viscosity, velocity, and bulk viscosity variation are sensed, are shown in Figure 24. In this part, the mentioned parameters vary for the water layer to track the effects of the resonant frequency. The values of the water properties are extracted from [38], while the temperature effect is not considered in the FEM simulations. Case #2 is the reference case representing water properties at room temperature (25 °C).

Table 4: Parameter values for water for three selected cases

<i>Cases</i>	$\eta_w(\text{mPa}\cdot\text{s})$	$\rho_w(\text{kg}\cdot\text{m}^{-3})$	$V(\text{m}\cdot\text{s}^{-1})$	$\mu(\text{mPa}\cdot\text{s})$
1	1.1400	998.97	1465.96	3.38
2	0.8880	997.00	1496.73	2.47
3	0.6527	992.22	1528.89	1.48

The simulations are performed with small step sizes around the resonant frequency peak to detect the frequency shift with better accuracy.

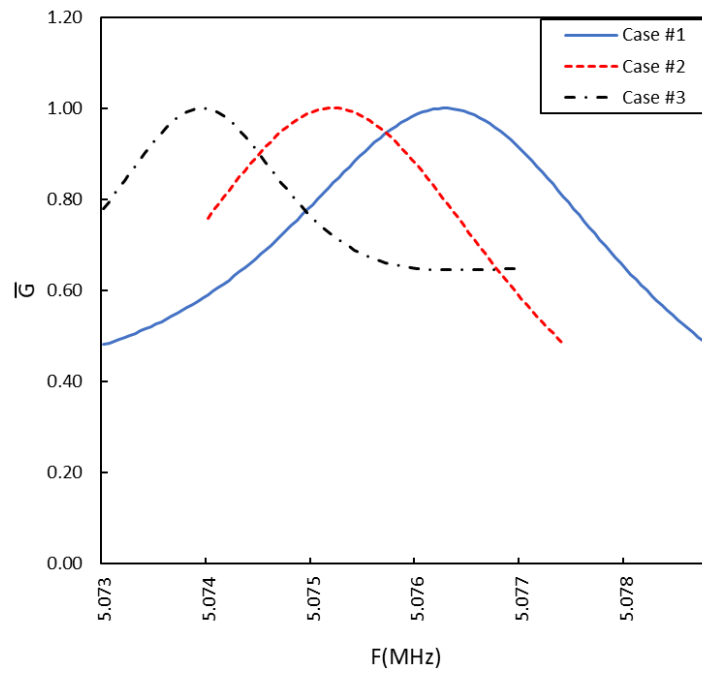
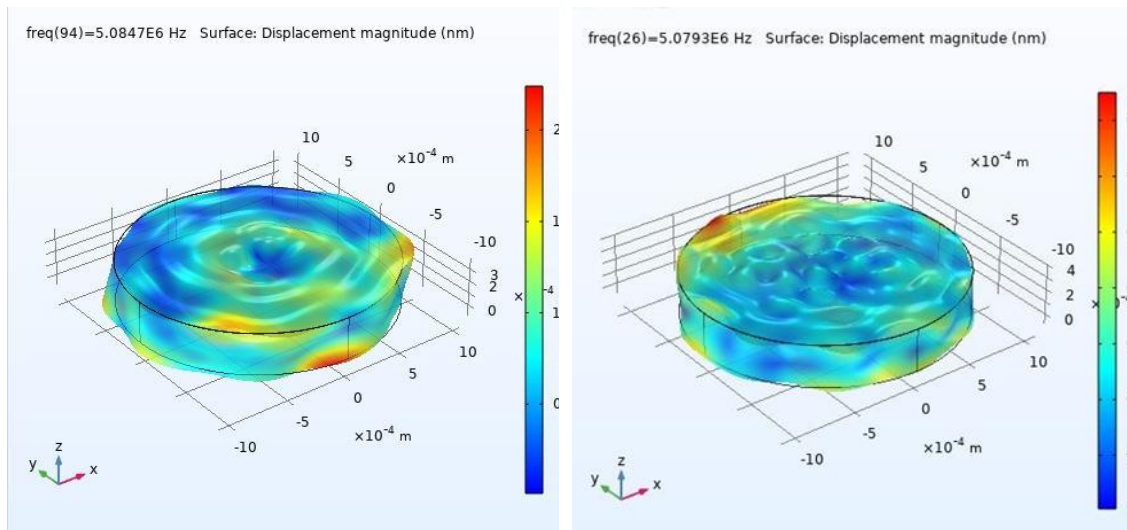


Figure 24: Resonant frequency of the QCM with respect to changing water layer properties (COMSOL results)

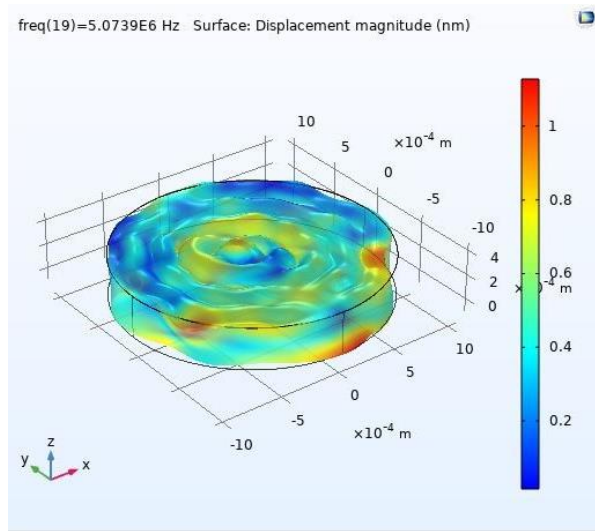
The resonant frequency of the QCM considering the first case is 5.084 MHz, the second case is 5.079 MHz, and the third case is 5.073 MHz. We observe a negative frequency shift of the operating frequency upon changes.

The displacement figures for each case are presented in Figure 25:



(a) Case #1

(b) Case #2



(c) Case #3

Figure 25: QCM displacement response (COMSOL results)

From displacement results, we observe that the shear characteristics of the mode are disturbed. The turbulence intensity is increased from case #1 to case #3.

### 3.4.1 Bulk viscosity and density sensing

To focus on the effect of bulk viscosity and density variation, four other cases are defined according to the below table. Case #3 is the reference case which represents water properties at room temperature (25 °C). In this part, only the bulk viscosity and density of the water are changing while other parameters are kept constant.

Table 5: Parameter values of water for four selected cases

Cases	$\eta_w$ (mPa. s)	$\rho_w$ (kg. m <sup>-3</sup> )	$V$ (m. s <sup>-1</sup> )	$\mu$ (mPa. s)
1	1.3100	999.70	1496.73	2.47
2	1.1400	998.97	1496.73	2.47
3	0.8880	997.00	1496.73	2.47
4	0.6527	992.22	1496.73	2.47

The simulation results around the peak are presented in the following graph.

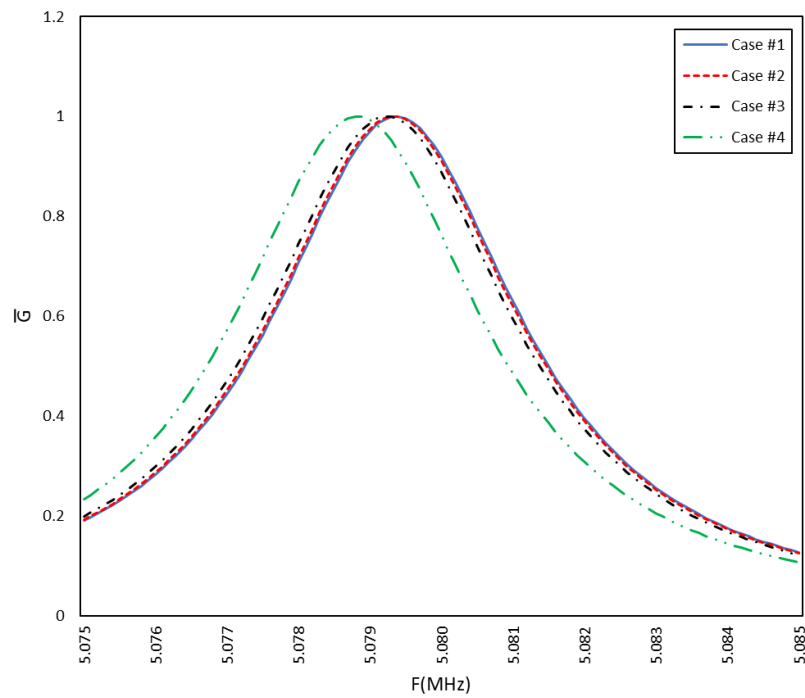


Figure 26: Resonant frequency of the QCM with respect to changing viscosity and density (COMSOL results)

From the results, we observe a negative shift of roughly 100Hz and 500 Hz for cases #1, #2,#3, and case #4, respectively, with regards to the changes in density and viscosity of the water. The absolute value of the frequency shift is comparable to the results from BVD circuit simulations in MATLAB and experimental data; however, the direction of the shifts is not positive, which is not appreciable.

## 4 Discussion

This section deals with the discussions about the models and obtained results. We will go through the details of the model and some comparisons between the real device and the achieved results.

### 4.1 Electrical equivalent model in MATLAB

The electrical equivalent model of the system (BVD), which is simulated in MATLAB, is fully comparable to the literature [33]. The applied characterization equations in the MATLAB codes give us the traceability of the effects of changes in each parameter with considerable precision. The model converges quickly, which makes it even more efficient.

As mentioned in the previous section, the achieved results are also aligned with the real device experiment data.

The BVD model fairly predicts the resonant frequency of the device in contact with air. The small deviation that we see can be related to the effect of  $C_0$ , which is not compensated in the BVD model while it is eliminated in the real device. Plus, there are some losses consolidated with the electric potential applied on the electrodes.

The electrical equivalent model represents an ideal device; hence we might not be able to see all the losses associated with the real measurements and spurious modes. Furthermore, in this thesis, the loading effect of the water layer is not considered. The temperature effect cannot be implemented directly into the model; however, the parameters used in characterization equations should be adjusted accordingly to see the effects as it is done in the analysis.

### 4.2 FEM analysis model in COMSOL

QCM is a widely used device in liquid sensing, as described in section one. COMSOL is a powerful tool for FEM simulations to predict the device's behavior, making it possible to simulate the factors that are not possible to consider in MATLAB simulation. In COMSOL models, there are limitations associated with device geometry, like the time consumption and the amount of process for each simulation. The modeled QCM provides the basis for the more complicated experiments. In many ways, the result of this work is detailing the

effect of some parameters like area, identifying different modes, loading of electrodes, density, and viscosity in sensing and measurement results.

For the sake of optimization, each layer is designed as a cylinder, while in a real device, the electrodes do not cover the whole sensor. Adding that, the sensitivity and overall performance of the QCM can be strongly affected by the device geometry; thus, the model accuracy is examined by optimizing the mesh and layers thickness.

The Sauerbrey equation predicted the loading effect of the gold electrode, and the model response is in line with the theory. The thickness-shear mode of the device is excited according to the results; however, we can observe spurious modes and other excited modes, which can affect the resonant frequency of the device in contact with liquid.

To establish a reliable sensing framework in liquid and performance optimization, the influence of water layer thickness on the device behavior is studied, which resulted in considering a thin layer of water with the thickness of  $1\mu\text{m}$ . From FEM results, we can see that the resonant frequency shifts more than what we achieved in MATLAB results. This can be due to the loading effect of the water layer, which we have not considered in the electrical equivalent model. Other factors like the thickness of each layer, natural vibration modes of the quartz, etc., can influence the results also. We examined a thicker layer of water which led to even bigger shifts. The thicker the liquid layer, the more the losses.

Consequently, the quality factor of the device drops down with increased losses. The suitable practice is to consider the highest quality factor, which happens where the liquid layer is thin. It is possible to consider compensation methods to reduce losses if a thicker layer of the water is implemented.

The FEM simulations provide the possibility of tracking changes in the characteristics of each layer separately. From BVD simulations, we were expecting to see small frequency shifts with respect to the variation in bulk viscosity and density of the liquid, which is confirmed by the FEM simulation; however, the shifts are in the opposite direction, which is not appreciated. This can be related to the boundary condition set in the pressure acoustic module for the water layer. We tried considering the water layer as a linear elastic material and redo the simulations; however, it did not conclude the desired results.

To summarize, this work provides the basics of the QCM model and behavior for further investigations. More parameters like temperature variation, the dynamic viscosity of the liquid layer, mass loading, damping coefficients, loss factors, etc., that affect the model performance, yet we have not to check these in detail.

## 5 Conclusion and future work

The main result of this thesis is a detailed investigation of some parameter changes in the QCM performance in liquid sensing using an electrical equivalent model simulated in MATLAB and FEM analysis in COMSOL. We have provided a good background on QCM sensing and operating modes and applied equations concerned with each system function. Parameter's settings are described to provide a clear understanding of the model.

We have illustrated the device's behavior in contact with air and water from the BVD simulation. The model response is reliable and in line with the experimental data collected from a commercially in-use QCM200 device. The effect of device dimension is demonstrated in detail and compared to the real device size. Implemented characteristic equations can predict the effect of other parameters on the QCM response. Using this model, we can foresee how the system will react in case of temperature change, different liquids sensing, and changes in crystal dimension (thickness and area). The effect of the water layer's bulk viscosity and density variation is investigated, precisely estimating the real device response based on the experimental data.

This model can be a reference as an ideal system to investigate the QCM behavior further and be expanded considering different boundary condition, the mass loading effect, losses,  $C_0$  cancelation, another liquid sensing, and compensation methods on liquid viscosity and density variations.

The FEM analysis is performed to resemble the real operation condition of the commercially in-use QCM200 device. The model indicates the system response in contact with air accurately. However, liquid sensing characteristics need deeper dive. The shear mode nature of the resonant is clear in the results, while we can see other exciting modes when the liquid layer is implemented. The device's geometry is heavily affecting the device's performance, which we have performed simulations and proved how the change in the radius of the sensor could shift the frequency. Further, the quality factor of the device is related to the thickness of the liquid layer, for which we have optimized the design to get a higher quality factor.

The following bullets describe the main achievements of this thesis:

- Implementing characterizing equations in the MATLAB model, which provide the prediction on the QCM device behavior in practice
- The model provides the possibility of tracing the effect of each parameter change on the response separately
- The FEM analysis provides the effect of geometry change on the device frequency shift and proposes an optimized solution for further investigations.

The experiments conducted in the FEM analysis are the first initial exploration of the QCM model, in which we attempted to prepare the basics of the model for further investigation. Our first plan to extend the model is to achieve the ideal boundary condition for liquid sensing considering the real device operating condition. There are more opportunities to investigate the model in terms of temperature effect, losses, wave reflections from the edges, loss compensation methods, quality factor improvement, and sensitivity examinations regarding bulk viscosity and density.

While our model has its shortcomings, the issue of the in liquid sensing behavior in FEM analysis; we believe that the main aim of the thesis and preparing the grounds for the future work is successfully achieved. Most importantly, there are several research topics to pursue in this field in the near future.

## References

- [1] A. A. M. Bahar, Z. Zakaria, A. A. Isa, E. Ruslan, and R. A. Alahnomi, "A Review of Characterization Techniques for Materials' Properties Measurement Using Microwave Resonant Sensor," vol. 7, no. 2, p. 7, 2015.
- [2] R. W. Murray, R. E. Dessy, W. R. Heineman, J. Janata, and W. R. Seitz, Eds., *Chemical Sensors and Microinstrumentation*, vol. 403. Washington, DC: American Chemical Society, 1989. DOI: 10.1021/bk-1989-0403.
- [3] M. G. Valdés, A. C. Valdés González, J. A. García Calzón, and M. E. Díaz-García, "Analytical nanotechnology for food analysis," *Microchim. Acta*, vol. 166, no. 1–2, pp. 1–19, Jul. 2009, doi: 10.1007/s00604-009-0165-z.
- [4] O. A. Postolache, J. M. D. Pereira, and P. M. B. S. Girao, "Smart Sensors Network for Air Quality Monitoring Applications," *IEEE Trans. Instrum. Meas.*, vol. 58, no. 9, pp. 3253–3262, Sep. 2009, DOI: 10.1109/TIM.2009.2022372.
- [5] M. I. Mead *et al.*, "The use of electrochemical sensors for monitoring urban air quality in low-cost, high-density networks," *Atmos. Environ.*, vol. 70, pp. 186–203, May 2013, doi: 10.1016/j.atmosenv.2012.11.060.
- [6] European Commission. Joint Research Centre. Institute for the Protection and the Security of the Citizen., *Review of sensors to monitor water quality: ERNCIP thematic area "Chemical & biological risks in the water sector," deliverable D1 task 1*. LU: Publications Office, 2013. Accessed: Nov. 14, 2021. [Online]. Available: <https://data.europa.eu/doi/10.2788/35499>
- [7] Y.-R. Li and J. Chu, "Study of BOD Microbial Sensors for Waste Water Treatment Control," *Appl. Biochem. Biotechnol.*, vol. 28–29, no. 1, pp. 855–863, Mar. 1991, DOI: 10.1007/BF02922655.
- [8] M. Engin, A. Demirel, E. Z. Engin, and M. Fedakar, "Recent developments and trends in biomedical sensors," *Measurement*, vol. 37, no. 2, pp. 173–188, Mar. 2005, DOI: 10.1016/j.measurement.2004.11.002.
- [9] A. A. Zainuddin, A. N. Nordin, R. A. Rahim, and W. C. Mak, "Modeling of a novel biosensor with integrated mass and electrochemical sensing capabilities," in *2016 IEEE EMBS Conference on Biomedical Engineering and Sciences (IECBES)*, Malaysia, Dec. 2016, pp. 420–425. DOI: 10.1109/IECBES.2016.7843485.
- [10] T. Koschinsky and L. Heinemann, "Sensors for glucose monitoring: technical and clinical aspects," *Diabetes Metab. Res. Rev.*, vol. 17, no. 2, pp. 113–123, Mar. 2001, DOI: 10.1002/dmrr.188.
- [11] C. I. L. Justino, T. A. Rocha-Santos, A. C. Duarte, and T. A. Rocha-Santos, "Review of analytical figures of merit of sensors and biosensors in clinical applications," *TrAC Trends Anal. Chem.*, vol. 29, no. 10, pp. 1172–1183, Nov. 2010, DOI: 10.1016/j.trac.2010.07.008.
- [12] Y. Zhang, J. Luo, A. J. Flewitt, Z. Cai, and X. Zhao, "Film bulk acoustic resonators (FBARs) as biosensors: A review," *Biosens. Bioelectron.*, vol. 116, pp. 1–15, Sep. 2018, DOI: 10.1016/j.bios.2018.05.028.
- [13] M. Rodahl, F. Höök, and B. Kasemo, "QCM Operation in Liquids: An Explanation of Measured Variations in Frequency and Q Factor with Liquid Conductivity," *Anal. Chem.*, vol. 68, no. 13, pp. 2219–2227, Jul. 1996, DOI: 10.1021/ac951203m.
- [14] J. Du, G. L. Harding, J. A. Ogilvy, P. R. Dencher, and M. Lake, "A study of Love-wave acoustic sensors," *Sens. Actuators Phys.*, vol. 56, no. 3, pp. 211–219, Sep. 1996, DOI: 10.1016/S0924-4247(96)01311-8.

- [15] C. G. Juan, B. Potelon, C. Quando, and E. Bronchalo, "Microwave Planar Resonant Solutions for Glucose Concentration Sensing: A Systematic Review," *Appl. Sci.*, vol. 11, no. 15, p. 7018, Jul. 2021, DOI: 10.3390/app11157018.
- [16] J. Curie and P. Curie, "An oscillating quartz crystal mass detector," *Rendu*, vol. 91, no. 5, pp. 294–297, 1880.
- [17] GHz. Sauerbrey, "Use of quartz vibrator for weighting thin films on a microbalance," *Z. Phys.*, vol. 155, pp. 206–212, 1959.
- [18] R. Bechmann, "Frequency-Temperature-Angle Characteristics of AT-Type Resonators Made of Natural and Synthetic Quartz," *Proc. IRE*, vol. 44, no. 11, pp. 1600–1607, Nov. 1956, DOI: 10.1109/JRPROC.1956.274879.
- [19] S. K. Vashist and P. Vashist, "Recent Advances in Quartz Crystal Microbalance-Based Sensors," *J. Sens.*, vol. 2011, pp. 1–13, 2011, DOI: 10.1155/2011/571405.
- [20] F. N. Dultsev and E. A. Kolosovsky, "QCM Operating in Threshold Mode as a Gas Sensor," *Langmuir*, vol. 25, no. 20, pp. 12195–12200, Oct. 2009, DOI: 10.1021/la901725f.
- [21] V. A. Minh, L. A. Tuan, T. Q. Huy, V. N. Hung, and N. V. Quy, "Enhanced NH<sub>3</sub> gas sensing properties of a QCM sensor by increasing the length of vertically orientated ZnO nanorods," *Appl. Surf. Sci.*, vol. 265, pp. 458–464, Jan. 2013, DOI: 10.1016/j.apsusc.2012.11.028.
- [22] A. Rehman, A. Hamilton, A. Chung, G. A. Baker, Z. Wang, and X. Zeng, "Differential Solute Gas Response in Ionic-Liquid-Based QCM Arrays: Elucidating Design Factors Responsible for Discriminative Explosive Gas Sensing," *Anal. Chem.*, vol. 83, no. 20, pp. 7823–7833, Oct. 2011, DOI: 10.1021/ac201583c.
- [23] A. M. Cao-Paz, L. Rodríguez-Pardo, J. Fariña, and J. Marcos-Acevedo, "Resolution in QCM Sensors for the Viscosity and Density of Liquids: Application to Lead Acid Batteries," *Sensors*, vol. 12, no. 8, pp. 10604–10620, Aug. 2012, doi: 10.3390/s120810604.
- [24] B. Acharya, M. A. Sidheswaran, R. Yungk, and J. Krim, "Quartz crystal microbalance apparatus for study of viscous liquids at high temperatures," *Rev. Sci. Instrum.*, vol. 88, no. 2, p. 025112, Feb. 2017, DOI: 10.1063/1.4976024.
- [25] X. Huang, Q. Bai, Q. Zhou, and J. Hu, "The Resistance–Amplitude–Frequency Effect of In–Liquid Quartz Crystal Microbalance," *Sensors*, vol. 17, no. 7, p. 1476, Jun. 2017, DOI: 10.3390/s17071476.
- [26] D. Zheng, J. Shi, and S. Fan, "Design and Theoretical Analysis of a Resonant Sensor for Liquid Density Measurement," *Sensors*, vol. 12, no. 6, pp. 7905–7916, Jun. 2012, DOI: 10.3390/s120607905.
- [27] A. Ballato, "Equivalent circuits for resonators and transducers driven piezoelectrically," ARMY Lab Command Fort Monmouth NJ Electronics Technology AND Devices Lab, 1990.
- [28] S. Butterworth, "'On electrically-maintained vibrations,' Proceedings of the Physical Society of London, vol. 27, pages 410–424.1914".
- [29] K. S. Van Dyke, "The Piezo-Electric Resonator and Its Equivalent Network," *Proc. IRE*, vol. 16, no. 6, pp. 742–764, Jun. 1928, DOI: 10.1109/JRPROC.1928.221466.
- [30] W. P. Mason and R. N. Thurston, *Physical acoustics: principles and methods*. New York London: Academic Press, 1977.
- [31] S. J. Martin, V. Edwards. Granstaff, and G. C. Frye, "Characterization of a quartz crystal microbalance with simultaneous mass and liquid loading," *Anal. Chem.*, vol. 63, no. 20, pp. 2272–2281, Oct. 1991, DOI: 10.1021/ac00020a015.

- [32] K. Hashimoto, Ed., *RF Bulk acoustic wave filters for communications*. Norwood, Mass. ; London: Artech House, 2009.
- [33] Z. Parlak, C. Biet, and S. Zauscher, "Decoupling mass adsorption from fluid viscosity and density in quartz crystal microbalance measurements using normalized conductance modeling," *Meas. Sci. Technol.*, vol. 24, no. 8, p. 085301, Aug. 2013, DOI: 10.1088/0957-0233/24/8/085301.
- [34] J. F. Rosenbaum, *Bulk acoustic wave theory and devices*. Artech House Acoustics Library, 1988.
- [35] Z.-G. Huang and Z.-Y. Chen, "Analysis of Excitation and Dead Vibration Modes of Quartz Resonators," *Adv. Acoust. Vib.*, vol. 2014, pp. 1–9, Feb. 2014, DOI: 10.1155/2014/746847.
- [36] D. S. Ballantine, Ed., *Acoustic wave sensors: theory, design, and physico-chemical applications*. San Diego: Academic Press, 1997.
- [37] T. B. Hoang, B. T. Stokke, U. Hanke, E. A. Johannessen, and A. Johannessen, "Signal Amplification of a Gravimetric Glucose Biosensor Based on the Concanavalin A–Dextran Affinity Assay," *IEEE Sens. J.*, vol. 21, no. 4, pp. 4391–4404, Feb. 2021, DOI: 10.1109/JSEN.2020.3032647.
- [38] M. J. Holmes, N. G. Parker, and M. J. W. Povey, "Temperature dependence of bulk viscosity in water using acoustic spectroscopy," *J. Phys. Conf. Ser.*, vol. 269, p. 012011, Jan. 2011, DOI: 10.1088/1742-6596/269/1/012011.

## List of figures

Figure 1: Schematic of QCM crystal

Figure 2: Thickness shear mode

Figure 3:(a) Single resonant BVD, (b) Multi resonant BVD each motional arm corresponds to a resonance[32]

Figure 4: Butterworth–van-Dyke circuit representation of QCM (BVD)[31]

Figure 5: The modified BVD (mBVD) considering losses

Figure 6: Mode shapes[35]

Figure 7: Complete QCM setup consisting of QCM200 digital controller, QCM25 crystal oscillator, crystal holder, and three quartz crystal

Figure 8: Crystal holder components

Figure 9:(a) Contact surface of QCM (b) Liquid surface of QCM

Figure 10: Model geometry

Figure 11: Mesh optimization based on wavelength

Figure 12: QCM displacement response to mesh optimization (a)  $\lambda/4$ , (b)  $\lambda/8$ , (c)  $\lambda/16$

Figure 13: (a) Meshing structure of the piezoelectric layer (b) Meshing structure of the model.

Figure 14: Normalized conductance versus frequency

Figure 15: Susceptance versus frequency

Figure 16: Impedance versus frequency

Figure 17: (a) Impedance phase. (b) derivative of impedance phase

Figure 18: QCM response with electrode & without electrode

Figure 19: Surface displacement magnitude of the QCM (a) with the electrodes (b) without electrodes

Figure 20: Electric potential of the QCM with electrodes at resonant frequency (a) 3D view cut out (b) 2D view cut out

Figure 21: The effect of change in radius on the resonant frequency

Figure 22: Frequency change of the QCM devices with radius  $835\mu\text{m}$ ,  $3500\mu\text{m}$  obtained from BVD in MATLAB, and QCM200 reference data

Figure 23: QCM response in contact with water

Figure 24: Resonant frequency of the QCM with respect to changing water layer properties

Figure 25: QCM displacement response

Figure 26: Resonant frequency of the QCM with respect to changing viscosity and density

## List of Tables

Table 1: BVD circuit parameters of QCM200

Table 2: Values of BVD parameters for the device in contact with air

Table 3: Values of BVD parameters in contact with water (a) device radius 3500 $\mu\text{m}$  (b) device radius 835 $\mu\text{m}$

Table 4: Parameter values for water for three selected cases

Table 5: Parameter values of water for four selected cases

## Appendix

### Example code

```
clc;
clear all;
close all;
Rx=0; fs=5e6;
ws=2*pi*fs;

R1_Air=10;L1_Air=30e-3;C1_Air=33e-15;R2_Air=0;L2_Air=0;
R1_Water=10;L1_Water=30e-3;C1_Water=33e-
15;R2_Water=390;L2_Water=12.8e-6;
C0=20e-12;
t=0;
for f=5.0508e6:2e1:5.066e6
    t=t+1;
    w=2*pi*f;
    w1(t)=w;
    Y_Air(t)=1i*w*C0+1/(R1_Air+(L1_Air*w-1/(C1_Air*w))*1i);
    Y_Water(t)=1i*w*C0+1/((R1_Water+R2_Water)+((L1_Water+L2_Water)*w-
1/(C1_Water*w))*1i);
    Z_Air=1./Y_Air;
    phi_Air=atan(imag(Z_Air)./real(Z_Air));
    Z_Water=1./Y_Water;
    phi_Water=atan(imag(Z_Water)./real(Z_Water));
end
d_phi_Air=gradient(phi_Air);
max_d_phi_Air=max(d_phi_Air);
d_phi_Water=gradient(phi_Water);
max_d_phi_Water=max(d_phi_Water);
d_phi_Air_Normalized=d_phi_Air/max_d_phi_Air;
d_phi_Water_Normalized=d_phi_Water/max_d_phi_Water;
w1=w1/(2*pi*1e6);
max_Air=max(real(Y_Air));
max_Water=max(real(Y_Water));
G_Air_Normalized=real(Y_Air)/max_Air;
G_Water_Normalized=real(Y_Water)/max_Water;
max_BAir=max(imag(Y_Air));
max_BWater=max(imag(Y_Water));
B_Air_Normalized=imag(Y_Air)/max_BAir;
B_Water_Normalized=imag(Y_Water)/max_BWater;

figure(1)
plot(w1,G_Air_Normalized,'b','linewidth',1.5)
hold on
plot(w1,G_Water_Normalized,'-.r','linewidth',1.5)
ylabel('G^-^-')
legend('Air','Water')
xlabel('F (MHz)')

figure(2)
plot(w1,B_Air_Normalized,'b','linewidth',1.5)
ylim([-1 1])
hold on
plot(w1,B_Water_Normalized,'-.r','linewidth',1.5)

legend('Air','Water')
xlabel('F (MHz)')
ylabel('B^-^-')
```

```

figure(3)
plot(w1,log(abs(1./Y_Air)), 'b', 'linewidth',1.5)
hold on
plot(w1,log(abs(1./Y_Water)), '-.r', 'linewidth',1.5)
legend('Air', 'Water')
ylabel('logabs(Z)')
xlabel('F (MHz)')

Qs_Air=ws*L1_Air/(Rx+R1_Air);
Qs_Water=ws*(L1_Water+L2_Water)/(Rx+R1_Water+R2_Water);

msgbox(['Qs_air= ', num2str(Qs_Air), '    Qs_water= ', num2str(Qs_Water)])

figure(4)
plot(w1,phi_Air, 'b', 'linewidth',1.5)
hold on
plot(w1,phi_Water, '-.r', 'linewidth',1.5)
legend('Air', 'Water')
ylabel('\phi', 'FontSize',16)
xlabel('F (MHz)')

figure(5)
plot(w1,d_phi_Air_Normalized, 'b', 'linewidth',1.5)
hold on
plot(w1,d_phi_Water_Normalized, '-.r', 'linewidth',1.5)
legend('Air', 'Water')
ylabel("\phi^-^-", 'FontSize',12)
xlabel('F (MHz)')

```